Vitamin D inhibits NF-κB activation in B cells and controls the humoral immune response

vorgelegt von
Diplom-Ingenieurin
Kerstin Geldmeyer-Hilt
aus Holzminden

Von der Fakultät III - Prozesswissenschaften
der Technischen Universität Berlin
zur Erlangung des akademischen Grades
Doktor der Ingenieurwissenschaften
- Dr.-Ing. -
genehmigte Dissertation

Promotionsausschuss:
Vorsitzender: Prof. Dr. rer. nat. Peter Neubauer
Berichter: Prof. Dr. er. nat. Roland Lauster
Berichter: Prof. Dr. med. Margitta Worm
Berichter: Prof. Dr. rer. nat. Leif-Alexander Garbe

Tag der wissenschaftlichen Aussprache: 24.03.2011

Berlin 2011
D83

Für meine Familie

TABLE OF CONTENT

1. ABSTRACT

Within the last years vitamin D has been established as an important immunomodulator. Vitamin D insufficiency, that is common in westernized countries especially during the winter season, has been linked to many immune disorders including type-I diabetes, rheumatoid arthritis, systemic lupus erythematosus and allergic asthma.

In anti-CD40 and IL-4 stimulated human B cells, 1α,25-dihydroxyvitamin D_3 (calcitriol), the bioactive metabolite of vitamin D, inhibits ε-germline expression and IgE production. This is associated with reduced nuclear amounts of NF-κB p50. Since CD40 signaling results in NF-κB p50 activation and, in combination with IL-4, in subsequent class switch recombination to IgE, it was investigated by which mechanism calcitriol modulates NF-κB mediated activation of human naïve B cells.

Naïve B cells were predominantly targeted by calcitriol in comparison with memory B cells as shown by pronounced induction of the Vitamin D receptor target gene *cyp24a1*. Vitamin D receptor ligation with calcitriol resulted in a strongly reduced p105/p50 protein and mRNA expression in human naïve B cells. This effect was mediated by impaired nuclear translocation of p65 and consequently reduced binding of p65 to its binding site in the p105 promoter. The data indicate that vitamin D receptor ligation modulates NF-κB activation by interference with NF-κB p65 translocation and consequently p105 expression. Thus, the vitamin D receptor inhibits costimulatory signal transduction in naïve B cells, namely by reducing CD40 signaling.

A sufficient vitamin D status in insufficient individuals is re-established by supplementation with 25-hydroxyvitamin D_3 (25(OH)VD_3). Therefore, the impact of 25(OH)VD_3 was analyzed in CYP27B1$^{-/-}$ mice, which are not capable of synthesizing bioactive calcitriol from 25(OH)VD_3. The humoral immune response was altered; in particular IgE production was elevated in CYP27B1$^{-/-}$ mice before and after allergeneic sensitization. Additionally, these mice displayed reduced numbers of B cells, but also effector memory T cells. In accordance with enhanced specific IgE and IgG1 responses, the cutaneous hypersensitivity reaction induced with allergen was more pronounced in CYP27B1$^{-/-}$ mice than in wt controls. Thus, calcitriol is an important molecule for the control of B cell dependent humoral immune responses; and at least in part interference with the NF-κB pathway is involved.

2. ZUSAMMENFASSUNG

Während der letzten Jahre wurde Vitamin D als wichtiger Immunmodulator etabliert. Vitamin D-Insuffizienz tritt in westlichen Ländern vor allem während des Winters auf und wurde mit vielen Krankheiten des Immunsystems wie Typ-I Diabetes, Rheumatoider Arthritis, Systemischem Lupus Erythematosus und allergischem Asthma in Verbindung gebracht.

In anti-CD40- und IL-4-stimulierten B-Zellen hemmt 1α,25-Dihydroxyvitamin D_3 (Calcitriol), der bioaktive Metabolit des Vitamin D, die Expression des ε-Keimbahn-Transkripts und die IgE-Produktion. Dies ist mit einer reduzierten Menge an NF-κB p50 im Zellkern verbunden. Da die Signaltransduktion über CD40 in der Aktivierung von NF-κB p50 und, in Kombination mit IL-4, im Klassenwechsel zu IgE mündet, wurde in der vorliegenden Arbeit untersucht, über welchen Mechanismus Calcitriol die NF-κB-vermittelte Aktivierung humaner naiver B-Zellen moduliert.

Die Vitamin-D-Rezeptor (VDR)-Aktivierung war in naiven B-Zellen stärker ausgeprägt als in Gedächtnis-B-Zellen, wie durch die stärkere Induktion des VDR-Zielgens *cyp24a1* gezeigt wurde. Die Ligation des VDR mit Calcitriol führte zu einer starken Reduktion der p105/p50-Expression sowohl auf mRNA- als auch auf Proteinebene. Dieser Effekt wurde durch eine verminderte p65-Kerntranslokation und die daraus hervorgehende reduzierte Binding von p65 an den p105-Promotor hervorgerufen. Die in dieser Arbeit erhobenen Daten zeigen, dass die Ligation des VDR die NF-κB-Aktivierung moduliert durch die Beeinflussung der p65-Translokation und der daraus resultierenden Expression von p105. Somit vermindert der VDR die kostimulatorische Signaltransduktion über CD40 in naiven B-Zellen.

Vitamin D-Insuffizienz wird durch die Supplementierung mit 25-Hydroxyvitamin D_3 (25(OH)VD_3) behoben. Der Einfluss von 25(OH)VD_3 auf die Immunantwort wurde in CYP27B1$^{-/-}$-Mäusen, die nicht zu einer Verstoffwechselung dieser Vorstufe zu Calcitriol befähigt sind, untersucht. Die humorale Immunantwort war stark verändert. Der deutlichste Effekt zeigte sich bei der IgE-Produktion, die in CYP27B1$^{-/-}$-Mäusen vor und nach der allergenen Sensibilisierung erhöht war. Außerdem war die Anzahl der B-Zellen und der Effektor-Gedächtnis-T-Zellen in der Milz reduziert. Übereinstimmend mit der erhöhten spezifischen IgE- und IgG1-Immunantwort war die Allergen-induzierte kutane Hypersensitivitätsreaktion in CYP27B1$^{-/-}$-Mäusen stärker ausgeprägt als in den Wildtyp-Kontrollen. Folglich ist Calcitriol ein wichtiges

Molekül für die Kontrolle der B-Zell-abhängigen humoralen Immunantwort, wobei zum Teil eine Beeinträchtigung des NF-κB-Signalweges eine Rolle spielt.

3. INTRODUCTION

3.1. Vitamin D metabolism and physiology

Vitamin D (VD) actually is not a true vitamin, because, although vitamin D_3 can be obtained by nutritional uptake, it is mainly synthesized by ultraviolet B (UVB)-mediated photosynthesis from 7-dehydrocholesterol in the skin[1]. Therefore, vitamin D is a hormone. During exposure to sunlight, the UVB radiation (290-315 nm) is adsorbed by 7-dehydrocholesterol in the skin to form previtamin D_3, which is rapidly isomerized to vitamin D_3 (VD_3) by thermal energy[2] (Figure 1). VD_3 is bound to the vitamin D binding protein (DBP) in the plasma and transported to the liver, where the first of the two essential hydroxylation steps to form bioactive vitamin D take place. 25-hydroxyvitamin D_3 ($25(OH)VD_3$) is generated by 25-hydroxylases (CYP27A1, CYP2R1, CYP3A4 and CYP2J3) and circulates through the blood bound to DBP as the main storage metabolite. It is used to determine the body's vitamin D status as this form has a longer half-life (2-3 weeks) than 1α,25-dihydroxyvitamin D_3 (4 hours)[3]. 1α,25-dihydroxyvitamin D_3 (calcitriol) is the bioactive metabolite of vitamin D and is mainly produced in the proximal tubule cells of the kidney by the 1α-hydroxylase CYP27B1[4] by a tightly regulated hydroxylation step. The catabolism of calcitriol is catalyzed by CYP24A1 by 24-hydroxylation.

The major physiologic function of calcitriol is to maintain serum calcium and phosphorus levels to support most metabolic functions, neuromuscular transmission and bone mineralization[5]. In response to even slight hypocalcemia when calcium is used for one of the above mentioned processes, the parathyroid glands secrete parathyroid hormone (PTH) which subsequently activates CYP27B1 in the kidney, so that calcitriol is produced[4]. In parallel, PTH suppresses CYP24A1 activity and thereby prevents calcitriol from being metabolized. Consequently, calcitriol plasma levels are markedly elevated. Calcitriol initiates active intestinal calcium transport in the small intestine to replace calcium which has been taken out of the plasma. To prevent hypercalcemia, PTH is feedback repressed by calcitriol[6].

Additionally, calcitriol mobilizes calcium from the skeleton by activating osteoclasts, which in turn demineralize bone or activate the reverse transport of calcium from the bone fluid compartment to the plasma compartment.

During the process of intestinal calcium transport also phosphate is mobilized. To exclude excess phosphate, fibroblast growth factor (FGF23) is secreted by

osteoblasts under the dual control of calcitriol and elevated blood phosphate[6]. FGF23 elicits phosphaturia so that phosphate is excreted via the kidneys, and inhibits the activity of renal CYP27B1.

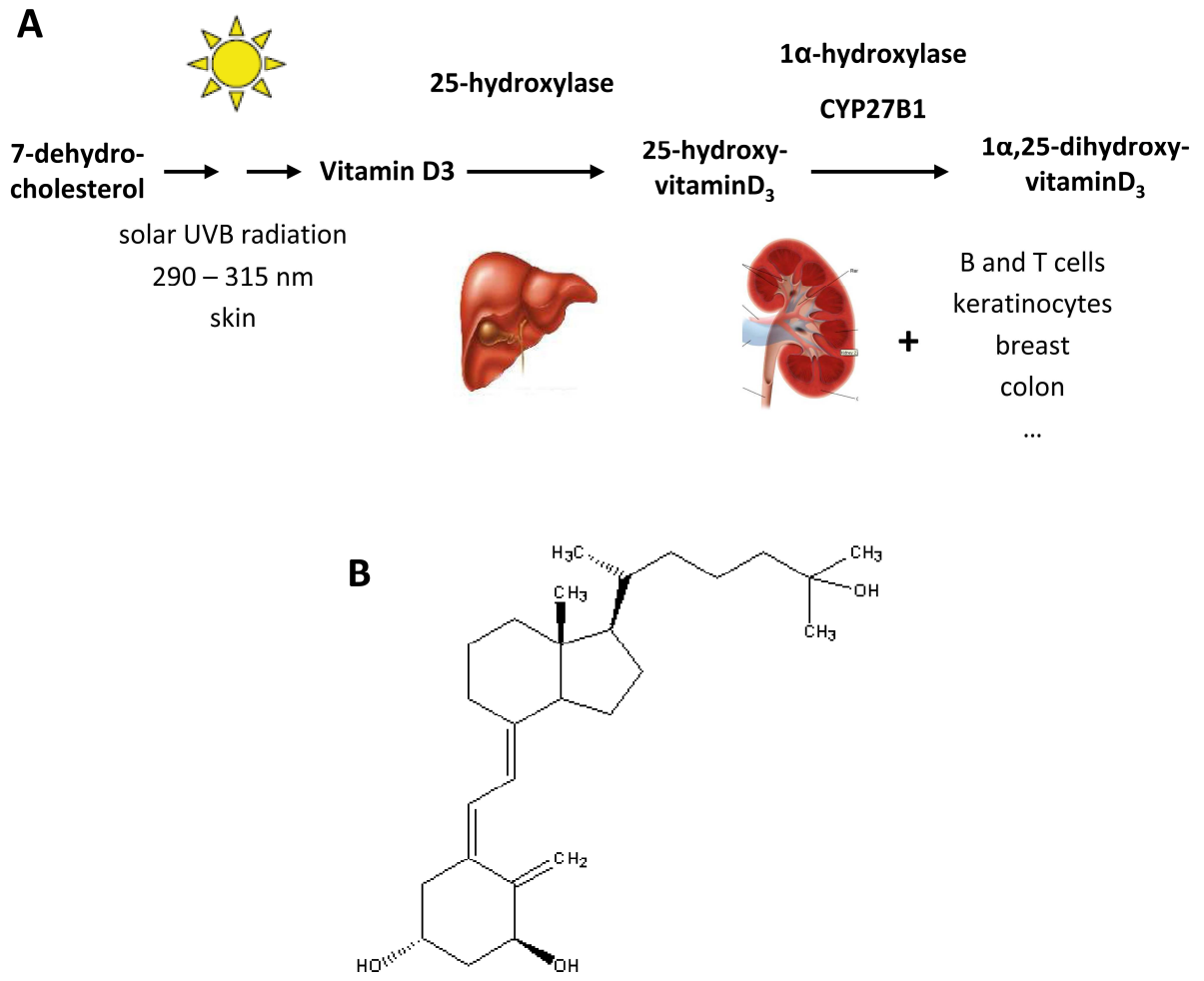

Figure 1. Vitamin D biosynthesis and structure. A. Vitamin D_3 is synthesized from 7-dehydrocholesterol in the skin after absorption of UVB. In the kidney, 25-hydroxylases catalyze the formation of the storage metabolite 25-hydroxyvitamin D_3. The last hydroxylation step to generate bioactive 1α,25-dihydroxyvitamin D_3 (calcitriol) typically occurs in the liver, but also in many other cell types including immune cells like B and T cells. **B.** Chemical structure of calcitriol.

3.2. Genomic actions of vitamin D

Calcitriol exerts its genomic actions via the vitamin D receptor (VDR), which belongs to the superfamily of nuclear hormone receptors and is a ligand-activated transcription factor. Its protein sequence is highly conserved between species.

The human VDR contains 427 amino acids and is a 48 kD protein. It comprises two major functional units: the N-terminal DNA binding domain (DBD) and the C-terminal ligand binding domain (LBD)[6] (Figure 2).

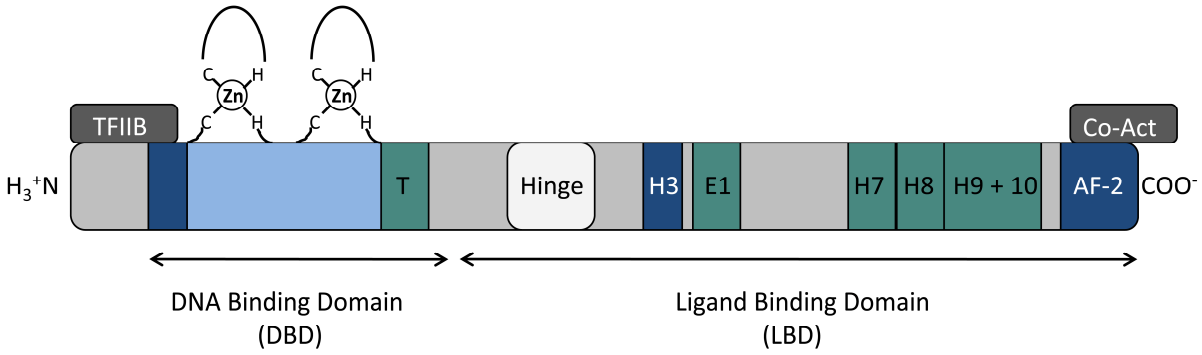

Figure 2. Fuctional domains of the vitamin D receptor. Zinc fingers are indicated in the DBD**.** H: α-helix, AF-2: activation function-2. Interaction sides with TFIIB and Co-Activators are indicated. Blue: transactivation. Green: heterodimerization with RXRs. Adapted from Haussler et al[6].

The DBD is the most conserved domain among nuclear hormone receptors and confers the ability to recognize specific target sequences and to activate genes[7]. It comprises eight cysteine residues that tetrahedically coordinate two zinc atoms to form zinc finger DNA binding motifs[8]. The DBD is rich in positively charged amino acids that favor electrostatic interactions with the negatively charged phosphate backbone of the DNA. The reverse β-turn adjacent to the second zinc finger, the so-called T-box, represents one of the dimerisation interfaces for retinoid X receptors (RXR).

The hinge region is not well conserved among the different nuclear receptors and allows rotation of the DBD and gives the VDR its conformational flexibility.

The LBD is a multifunctional domain that, in addition to the binding of ligand, mediates homo- and heterodimerisation, nuclear import signaling and interaction with the transcriptional machinery[7, 8]. Upon ligand-binding in the genomic ligand-binding pocket (LBP), the VDR undergoes a conformational change which allows for heterodimerisation and cofactor binding. Recently, the presence of an alternative LBP responsible for rapid non-genomic actions of the VDR has been demonstrated[9]. Modeling data suggest that both LBPs overlap, so that only one calcitriol molecule can occupy the VDR at any given time.

In the LBD 12 α-helical structures present VDR surfaces for heterodimerisation with RXRs as well as for transactivation via interaction with coactivators. The VDR also complexes with basal transcription factors such as TFIIB as well as with transcriptional corepressors such as the *hairless* (Hr) gene product, which associates with the VDR hinge region and α-helix H3[6].

The activation function (AF)-2 domain at the N-terminus of the VDR provides an interactive surface for transcriptional corepressors and coactivators which link VDR activity with the preinitiation complex[8].

About 0.5% (approximately 200 genes) of all genes in the human genome are estimated to be transcriptionally regulated by the VDR. However, by various mechanisms the VDR seems to be involved in the indirect regulation of even more genes[10]. Upon ligand binding the VDR heterodimerizes with RXR and translocates to the nucleus, where it binds to vitamin D responsive elements (VDREs) in the promoter regions of VD regulated genes. Alternatively VDR/RXR-complexes are present on the DNA in an unliganded state, but are transcriptionally inactive until calcitriol binding increases the affinity of VDR for DNA and promotes VDR binding specificity[11]. Calcitriol-unligated VDR/RXR heterodimers recruit corepressors with histone deacetylase activity, promoting repressive nucleosome configuration of the chromatin[12]. The AF-2 domain of the VDR is exposed only after the conformational change induced by calcitriol ligation. Corepressors such as nuclear receptor corepressor (NCoR) and silencing mediator for retinoid and thyroid hormone receptors (SMRT) are released[13] and coactivators such as steroid receptor coactivator-1, transcriptional intermediary factor-2 and nuclear receptor coactivator-3, which recruit CBP/p300, are bound instead. Alternatively, also calcitriol liganded VDR/RXR complexes can recruit NCoR and SMRT and thereby inhibit gene transcription[14]. Thus, although VDR/RXR complexes positively regulate gene expression in most cases, negative regulation does also occur.

VDREs usually share the consensus sequence RGKTSA (R=A or G, K=G or T, S=C or G)[8]. This hexameric sequence represents one half site, the complete VDRE comprises two half sites spaced by 3 nucleotides (DR3) or everted repeats spaced by 6–9 nucleotides (ER6 and ER9, respectively)[15]. The VDREs of most previously studied negatively regulated genes resemble those of positively regulated genes[16]. In contrast, the negative VDRE (nVDRE) of the CYP27B1 promoter is an exception,

because it does not contain a consensus sequence[17]. In addition, Murayama et al proposed that the regulation of the *cyp27b1* gene involves an indirect binding of the VDR to DNA, where the VDR associates with the nVDRE liganddependently via another transcription factor, the VDR interacting repressor (VDIR)[17, 18].

Besides mediating transcriptional regulation via the VDR calcitriol induces rapid, nongenomic responses, most likely by binding to its alternative binding pocket[9]. Additionally the existence of a plasma membrane calcitriol binding activity, now called the membrane-associated rapid response steroid binding (MARRS) protein, is also discussed[19]. One example of rapid VDR action is calcitriol-induced transcellular flux of calcium across the intestine (transcaltachia)[20].

3.3. Vitamin D and the immune system

In addition to being processed in the liver and kidney, VD_3 can also be metabolized by cells of the immune system, so that calcitriol is concentrated locally in lymphoid microenvironments[20]. Thereby, not only specific local actions are mediated, but also systemic side effects like hypercalcemia and increased bone resorption are limited. Activated B and T cells express CYP27B1 and can convert 25(OH)VD_3 to calcitriol[21, 22]. Macrophages as well as monocyte-derived and dermal dendritic cells (DCs) even express 25-hydroxylase[23] and thus can produce calcitriol from VD_3. CYP27B1 expressed in immune cells is identical to the renal enzyme, but the regulation of its expression and activity is different[24]. In macrophages, CYP27B1 is regulated by IFNγ and Toll-like receptor agonists[25] and not subjected to negative feedback signals from calcitriol.

In T cells, calcitriol stimulation blocks the induction of T-helper-1 (T_H1) cell cytokines like IFNγ, while promoting T_H2 cell responses by enhancing interleukin (IL)-4 production[20]. Proliferation is inhibited by a decrease in IL-2 production. VDR/RXRα inhibits NFATp/AP-1 complex formation and directly binds to the NFAT binding site in the IL-2 promoter in a sequence specific manner, thereby preventing NFAT to activate transcription[26, 27]. In the IFNγ promoter, liganded VDR/RXRα directly binds to a nVDRE and presumably interacts with a crucial upstream enhancer element[28]. Calcitriol augments T_H2 cell development by increasing the expression of the T_H2-specific transcription factors GATA-3 and c-maf, resulting in increased production of

IL-4, IL-5 and IL-10[29]. A contradictory study reports the inhibition of IL-4 transcription after *in vitro* calcitriol treatment of naïve $CD4^+$ T cells[30].
In antigen-presenting DCs and activated macrophages, calcitriol suppresses the synthesis of the T_H1-promoting cytokine IL-12 by downregulation of NF-κB-activity, which is prevented from binding to the κB regulatory element in the p40 promoter[31]. Due to this inhibition of IL-12, observed *in vitro* as well as *in vivo*, calcitriol interferes directly with a key event in the immune cascade shifting the ongoing reaction away from a T_H1 and towards a T_H2 profile. In addition, expression of the immunosuppressive cytokine IL-10, opposing the T_H1 driving effects of IL-12, is increased in DCs by treatment with calcitriol[32]. DCs are the primary initiators of T cell mediated immune responses *in vivo* and, when fully mature, express high levels of class II MHC, CD80, CD86 and CD40. Calcitriol induces a tolerogenic phenotype by decreasing the expression of these costimulatory surface molecules[33, 34].
Additionally, $CD4^+$ $CD25^+$ T_{reg} are increased by calcitriol as shown by increased FoxP3 expression and IL-10 production in humans as well as in mice[35, 36].

In line with the T_H1 suppressive effects of calcitriol, low $25(OH)VD_3$ serum levels have been associated with primarily T_H1 mediated diseases including type-I diabetes[37], multiple sclerosis[38], rheumatoid arthritis[39] and inflammatory bowl disease[40]. In case of acute allergic asthma, which is driven by the T_H2-related cytokine IL-4, the influence of vitamin D is discussed controversially and probably dependent on the timing and dose of exposure[41]. In one study of murine allergic asthma, calcitriol administration inhibited airway inflammation and decreased IL-4 levels in bronchoalveolar lavage fluids[42]. However, in a different study, vitamin D enhanced IL-4, IL-13 and IgE when given early during sensitization, but inhibited IL-5 and airway eosinophilia when administered later[43]. In a human study a nonlinear relationship between serum $25(OH)VD_3$ and IgE was found, with low as well as high titers of $25(OH)VD_3$ correlating with enhanced IgE levels[44]. Asthmatic children from Costa Rica displayed a correlation between low vitamin D levels and asthma severity[45].

Besides its inhibitory effect on T cells, calcitriol has various effects on B cells. It decreases B cell proliferation, plasma-cell differentiation and IgG secretion[22]. Previous data show that calcitriol inhibits IgE production in human peripheral B cells, most likely by modulating the NF-κB p50 activation[46]. Additionally, ligand activated

VDR binds to the ε-germline promoter as a complex with RXRα and recruits SMRT corepressors, but also histone deacetylase (HDAC)-1 and 3[47].

Interestingly, calcitriol inhibits mitogen stimulated IgG production by B cells from patients with inactive systemic lupus erythematosus (SLE), but not the spontaneous IgG production by cells from patients with active SLE[20]. Thus, it is possible that fully differentiated memory B cells and/or antibody-secreting cells (ASCs) are refractory to calcitriol. Remarkably, $25(OH)D_3$ serum levels are significantly reduced in SLE patients, a disease which is characterized by immune dysregulation resulting in overproduction of autoantibodies, leading to the hypothesis that calcitriol may be important in maintaining B cell homeostasis[22]. The effects of calcitriol on several immune cell-types are summarized in Figure 3.

Ablation or impairment of endogenous calcitriol synthesis have been associated with immune defects resembling those associated with low serum $25(OH)VD_3$ levels. A rickets causing mutation in the gene expressing *cyp27b1* has been identified as a risk factor for multiple sclerosis[48]. A promoter polymorphism of the *cyp27b1* gene has been associated with autoimmune diseases like Addison's disease, Hashimoto's thyroiditis, Graves' disease and type-I diabetes mellitus[49]. However, the immunological relevance of the targeted ablation of CYP27B1 in mice has not been well characterized yet. Only Panda et al observed reduced numbers of peripheral $CD4^+$ and $CD8^+$ T cells[50].

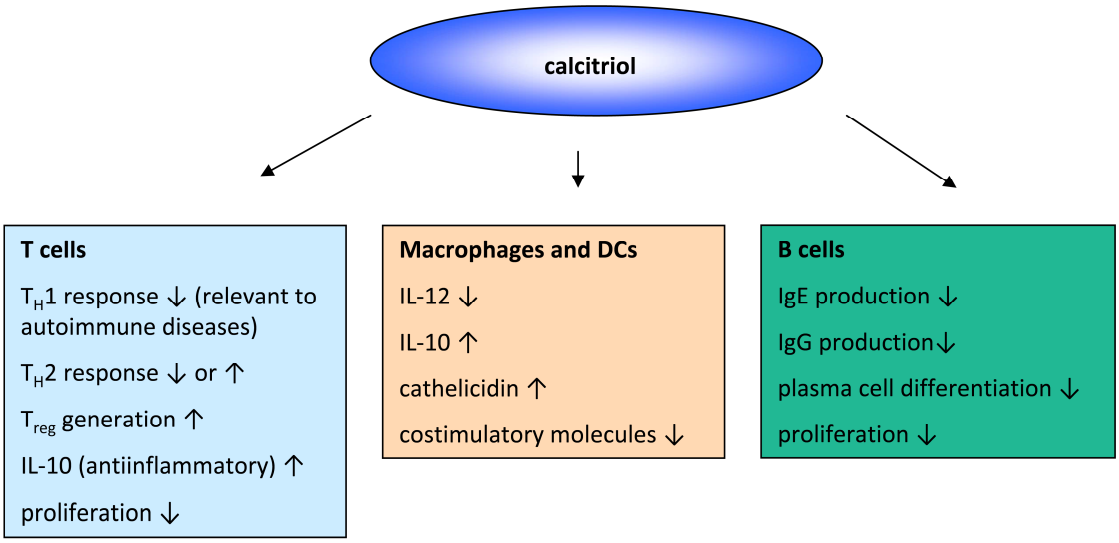

Figure 3. Calcitriol and the immune system. Systemically or locally produced calcitriol exerts its effects on several immune-cell types, including macrophages, DCs, T and B cells. Adapted from Mora et al[20] and Lange et al[41].

3.4. The NF-κB family of transcription factors

Nuclear factor (NF)-κB transcription factors can both induce and repress gene expression by binding to DNA sequences named κB elements in the promoter regions of certain genes. In mammals the family of NF-κB includes five members, namely, RelA (p65), RelB, c-Rel, p105 (NF-κB1) and p100 (NF-κB2)[51, 52]. p105 and p100 are posttranscriptionally processed to the DNA binding subunits p50 and p52, respectively[53]. Different NF-κB complexes can be formed from their homo- and heterodimers, which are retained in the cytoplasm of unstimulated cells by inhibitors of NF-κB (IκBs). The family of IκBs principally comprises IκBα, IκBβ, IκBε and Bcl-3[54]; p105 and p100 contain an intrinsic IκB activity. NF-κB can be activated by different stimuli and generally results in phosphorylation of IκB by the IκB kinase (IKK) complex, which results in IκB degradation by the 26S proteasome. Degradation of ubiquitinated IκBα occurs rapidly, whereas degradation of IκBβ and IκBε is delayed, or sometimes does not occur at all[55-57]. NF-κB dimers are released and translocate to the nucleus where they act as transcription factors. Depending on the stimulus, different pathways of NF-κB, mainly the canonical and the alternative pathway, are activated resulting in nuclear translocation of distinct NF-κB dimers[51, 54].

In B cells the surface molecule CD40 mediates important functions like the regulation of B cell proliferation, production of immunoglobulins, immunoglobulin class switching, rescue of B cells from apoptotic death, germinal center formation, and generation of B cell memory[58, 59].

CD40 signaling strongly activates both, the canonical and the alternative NF-κB pathway in B cells[60] mediated by tumor-necrosis factor receptor (TNFR)-associated factor (TRAF)-1, 2, 3 and 6[61] (Figure 4). The canonical NF-κB-pathway involves the activation of the IKK complex, which typically consists of the catalytic subunits IKKα and IKKβ and the regulatory subunit IKKγ (NF-κB essential modulator, NEMO)[51]. The activated IKK complex catalyzes the phosphorylation of IκBs, polyubiquitinylation and subsequent degradation by the 26S proteasome. Most commonly, p50/p65 dimers, but also p50/c-Rel dimers are released to translocate to the nucleus. NF-κB activation via the canonical pathway is a rapid process, while activation via the alternative pathway is more sustained. Following stimulation of the alternative pathway, TRAFs activate NF-κB inducer kinase (NIK) to phosphorylate dimers of IKKα, which in turn phosphorylate p100[60]. As an inhibitor of κB p100 retains its

dimerisation partner RelB in the cytosol. Upon phosphorylation p100 is processed to p52, so the p52/RelB dimers translocate to the nucleus.

While noncanonical NF-κB activation via CD40 mediates cell survival in B cells, proliferation and isotype switching depend mostly on canonical NF-κB activity[62, 63].

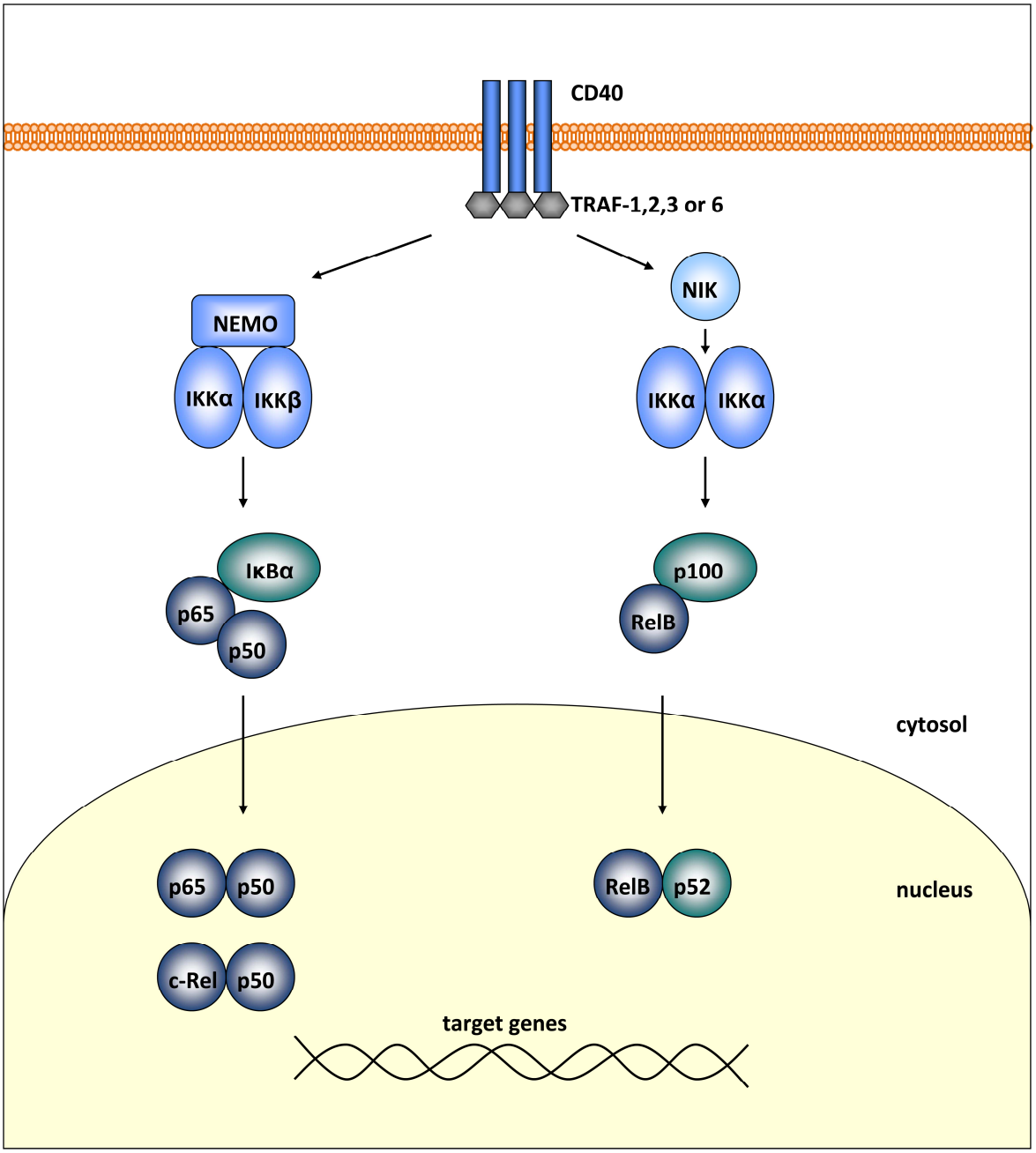

Figure 4. CD40 signaling activates the canonical and the alternative NFkB pathway. Adapted from Sun et al[64].

4. AIMS OF THIS STUDY

Within this thesis, the well known immunomodulatory properties of VD were subject of detailed analysis, mainly within the B cell compartment.

1α,25-dihydroxyvitamin D_3 (calcitriol), the bioactive metabolite of vitamin D, modulates the activation and inhibits IgE production of anti-CD40 and IL-4 stimulated human peripheral B cells. Engagement of CD40 results in NF-κB p50 activation, which is essential for the class switch to IgE. In this thesis, it was investigated by which mechanism calcitriol modulates NF-κB mediated activation of human naïve B cells.

Since it has been proposed that mean serum concentrations of 25(OH)VD_3, especially during the winter season, are not high enough to maintain the immunological functions of VD, many scientists being active in this field recommend supplementation with 25(OH)VD_3. 25(OH)VD_3 is the so called storage metabolite of VD, because it has a longer half-life and is metabolized to calcitriol if needed. To analyze the impact of 25(OH)VD_3 *in vivo*, the type-I immune reaction was analyzed in CYP27B1$^{-/-}$ mice which lack the enzyme responsible for the generation of calcitriol out of its precursor. Focus of these analyses was the humoral immune response in the context of an allergic sensitization and according to that a detailed assessment of the responsible B and T cell compartments.

5. MATERIAL

5.1. Chemicals and reagents

Chemical	Supplier
Acryl amide, 30 %	Roth
Advanced RPMI 1640	Invitrogen
Albumin from chicken egg white, Gade V	Sigma-Aldrich
avidin/biotin blocking kit	Vector Labs
3-Amino-9-ethyl-carbazole (AEC)	Sigma-Aldrich
Ammunium persulfat (APS)	Sigma-Aldrich
Beta-mercaptoethanol	Sigma-Aldrich
Bovine serum albumine (BSA), pH 7.0	SERVA
Citric acid, $C_6H_8O_7$	Merck
charcoal stripped fetal calf serum	Biochrom
Complete Protease Inhibitor	Roche
Developer, G153	AGFA
n,n-Dimethyl formamide (DMF)	Sigma-Aldrich
Disodium hydrogen phosphat, Na_2HPO_4	Merck
DNAse	Macherey-Nagel
Diethanol amine, $(HOCH_2CH_2)_2NH$	Sigma-Aldrich
ECL High performance Chemiluminescence film	Amersham
ECL Plus Western Blot Detection Reagents	Amersham
ExtrAvidin-Peroxidase (SA-HRP)	Sigma
FastStart DNA Master SYBR® Green	Roche
Fetal calf serum (FCS)	Biochrom
Ficoll, sterile, d = 1,077 g/mL	PAA
Glycine	SERVA
Hydrochloric acid, HCl , 25%	Merck
Hydrogen peroxide, H_2O_2, 30%	Merck
Imject Alum	Amersham Pierce
Recombinant human Interleukin (IL)-4	Miltenyi Biotec
Ketamin hydrochloride	Actavis
L-glutamine	Biochrom
M column	Miltenyi Biotec
Magnesium chloride, $MgCl_2$	Merck
Methanol C_2H_5OH	Merck
µMACS column	Miltenyi Biotec
Milk powder (Blotting Grade)	Roth
Mouse Regulatory T cell Staining Kit 3	eBioscience
Multiscreen hts ip hydrophobic PVDF 0.45 µm	Millipore

NE-PER™ Extraction Reagents	Pierce
NovaBlue substrate kit	Vector Labs
NovaRed substrate kit	Vector Labs
Nucleospin Extract II	Macherey-Nagel
Nucleospin RNA II Kit	Macherey-Nagel
Paraformaldehyde (PFA)	Sigma-Aldrich
Para-Nitrophenyl phosphate	Sigma-Aldrich
Dulbecco´s PBS without Ca2+/Mg2+, sterile	PAA
penicillin	Biochrom
Physiological saline, 0.9 % NaCl	Braun
Potassium chloride, KCl	Merck
Potassium dihydrogen phosphat, KH_2PO_4	Merck
Precision Plus Protein Standard Dual Color	Bio-Rad
Protein A-coupled magnetic microbeads	Miltenyi Biotec
Proteinase K	Macherey-Nagel
Rapid Fixer, G153	AGFA
Reverse Transcription Kit	Applied Biosystems
Rompun 2% (Xylazinhydrochlorid)	Bayer Health Care
RPMI 1640, without Ca2+/Mg2+, sterile	Biochrom
Salmon sperm DNA	Invitrogen
Saponin	Sigma-Aldrich
Sodium carbonate, Na_2CO_3	Merck
Sodium chloride, NaCl	Merck
Sodium dodecyl sulfate (SDS)	Sigma-Aldrich
Sodium hydrogen carbonate, $NaHCO_3$	Merck
Streptavidin-HRP, 100µg/mL	R&D
Streptavidin-AP	ZYMED
streptomycin	Biochrom
Sulphuric acid, H_2SO_4, 95-97%	Riedel de Haen
Tetramethyl benzidine dihydrochloride, TMB	Sigma-Aldrich
Tetramethyl ethylene diamine (TEMED) $C_6H_{16}N_2$	Bio-Rad
Tris(hydroxymethyl)aminomethane (Tris-Base)	Sigma-Aldrich
Tween20	Bio-Rad
Vector Mount medium	Vector labs

5.2. Buffers and solutions

Buffer	Recipe
AEC substrate buffer	7.5 ml 0.2 M acetic acid 10.55 ml 0.2 M Sodium acetate 15 ml H_2O_{bidest}
AEC solution	1 tablet of 3-amino-9-ethyl-carbazole (AEC) is resolved in 2 ml N,N-dimethyl- formamide (DMF). 1 ml of AEC-DMF solution is added dropwise into 33,05 ml substrate buffer 12 µl H_2O_2 are added to 22 ml substrate solution
AP substrate buffer	9.7% (v/v) diethanolamine, 0.1 mM $MgCl_2$
ChIP dilution buffer	16.7 mM Tris-HCl pH8, 167 mM NaCl, 1.1% Triton X-100, 1.2 mM EDTA
ChIP elution buffer	1% SDS, 0.1 M $NaHCO_3$
FACS buffer	PBS/1% BSA
high salt buffer	0.1% SDS, 1% Triton X-100, 2 mM EDTA, 500 mM NaCl, 20 mM Tris-HCl pH=8.1,
MACS buffer	PBS/0.5% BSA/2mM EDTA
LiCl buffer	0.25 M LiCl, 1% NP40, 1% sodium deoxycholate, 1 mM EDTA, 10 mM Tris-HCl pH=8.1
low salt buffer	0.1% SDS, 1% Triton X-100, 2 mM EDTA, 150 mM NaCl, 20 mM Tris-HCl pH=8.1,
PBS	137 mM NaCl, 2.7 mM KCl, 10 mM Na_2HPO_4, 18 mM KH_2PO_4, pH 7.4
SDS lysis buffer	1% SDS, 10 mM EDTA, 50 mM Tris, pH= 8.1
separating gel (5%)	5 % v/v Acrylamide, 0.125 M Tris, 0.1% (w/v) SDS, 0.1% (v/v) APS, 0.01 % v/v TEMED
sodium carbonate buffer	45 mM $NaHCO_3$, 9.1 M Na_2CO_3 pH 9

stacking gel (12%)	12% (v/v) Acrylamide, 0.5 M Tris, 0.1% (v/v) SDS, 0.1% (v/v) APS, 0.04% (v/v) TEMED
TE	10 mM Tris-HCl pH=8.1, 1 mM EDTA pH=8.0
TMB substrate buffer	51.4 mM Na2HPO4, 24.3 mM citric acid, pH 5.5
Western blot running buffer	192 mM glycine, 24.8 mM Tris, 0.1% (w/v) SDS
Western blot sample buffer (5x)	250 mM Tris pH 6.8, 10% SDS, 50% glycerol, 0.02% bromphenol blue, add 10% beta-mercaptoethanol prior to use
Western blot transfer buffer	192 mM glycine, 24.8 mM Tris, 20% (v/v) methanol

5.3. Antibodies and secondary reagents

antibody	clone / designation	manufacturer
anti-human βActin	4967	Cell Signaling
anti-human CD14	magnetic beads	Miltenyi Biotec
anti-human CD14 FITC	MφP9	BD
anti-human CD19 PE	LT19	Miltenyi Biotec
anti-human CD19	magnetic beads	Miltenyi Biotec
anti-human CD20 FITC	2H7	eBioscience
anti-human CD27	magnetic beads	Miltenyi Biotec
anti-human CD27 PE	2G.7F9	eBioscience
anti-human CD27 APC	M-T271	Miltenyi Biotec
anti-human CD40	626	Santa Cruz Biotechnology
anti-human IκBα Alexa Flour 647	L35A4	Cell Signaling
anti-human NFκB1	rat monoclonal	Lifespan Biosciences
anti-human nucleolin	N662	Sigma-Aldrich
anti-human p65	20/NFκB/p65	BD
anti-human p65	C-20	Santa Cruz Biotechnology
anti-human VDR	9A7	Affinity Bioreagents
anti-mouse B220 FITC	RA3.6B2	DRFZ
anti-mouse B220 pacific blue	RA3.6B2	DRFZ
anti-mouse CD138 PE	281-2	BD
anti-mouse CD19 APC	ID3	BD
anti-mouse CD21 FITC	7G6	BD
anti-mouse CD23 PE	B3B4	BD

anti-mouse CD25 PE	PC 61.5	eBioscience
anti-mouse CD3ε FITC	145-2C11	eBioscience
anti-mouse CD4 FITC	RM4-5	eBioscience
anti-mouse CD4 PE	GK1.5	DRFZ
anti-mouse CD44 PE-Cy7	IM7	eBioscience
anti-mouse CD62L Alexa405	MEL14	DRFZ
anti-mouse CD8 APC	53.7	eBioscience
anti-mouse Fcγ receptor	2.4G	DRFZ
anti-mouse FoxP3 PE-Cy5	FJK-16s	eBioscience
anti-mouse IgA biotin	1040-08	Southern Biotech
anti-mouse IgD biotin	11.26c	DRFZ
anti-mouse IgG1 APC	X56	BD Pharmingen
anti-mouse IgG1 biotin	A85.1	BD Pharmingne
anti-mouse IgM Alexa405	M41	DRFZ
anti-mouse MOMA-1 biotin	T-2021	BMA Biomedicals
anti-FITC-HRP		Sigma-Aldrich
anti-mouse-HRP	goat, sc-2005	Santa Cruz Biotechnology
anti-rabbit-HRP	goat, sc-2004	Santa Cruz Biotechnology
anti-rat HRP	goat, sc2006	Santa Cruz Biotechnology
ProteinA microbeads	magnetic beads	Miltenyi Biotec
SA-AP	ExtrAvidin Phosphatase	Sigma-Aldrich
SA-HRP (ELISPOT)	ExtrAvidin-Peroxidase	Sigma-Aldrich
SA-HRP (ELISA)	AEM 6208122	R&D
SA-PE-Cy7		BD Pharmingen

5.4. Lab ware and commodities

Lab Ware	Supplier
6 Well plates, sterile, suspension	Greiner
24 Well plates, sterile, suspension	Greiner
48 Well plates, sterile, suspension	Greiner
96 Well plates, sterile, suspension	Greiner
96 Well plates (ELISA) Maxi sorb	NUNC
96 Well plates, sterile (ELISPOT) 0.45 High Protein Binding Immibilion-P Membrane	Millipore
Cover slips	Menzel-Gläser
Disposable vinyl specimen Cryomold Tissue-Tek	Sakura
Light Cycler Capillaries	Roche
Liquid Blocker Pap Pen	Kisker-Biotech

LS columns	Miltenyi Biotec
M columns	Miltenyi Biotec
µ columns	Miltenyi Biotec
Maxisorp 96 well plates	NUNC
Microscope slides Super frost plus R.	Langenbrinck
O.C.T. medium Tissue-Tek	Sakura
Ophthalmic gel Vidisic	Bausch & Lomb
Protean3 system	Bio-Rad
Scalpel, sterile No. 20	Feather
Syringes, sterile 10ml, 20 ml, 50ml	Braun
Western Blot Cassette ECL Hypercassette	Amersham
Western Blot Membrane Polyvinylidenfluorid (PVDF)	Amersham
Whatman Paper	Schleicher & Schuell

Reaction tubes, pipette tips and other commodities were used from Eppendorf, Falcon, and Sarstedt.

5.5. Technical Equipment

Equipment	Model	Manufacturer
Autoclave		MELAG
Centrifuge	Megafuge 1.OR	Heraeus
	Multifuge 4KR	Heraeus
	5417R; 5417R	Eppendorf
	Minifuge RF	Heraeus
Cryostat	Jung frigocut 2800N	Leica
Electronic cell counter	CASY 1, Modell TT	Innovatis
ELISA reader	Dynex MRX version 1.33	DYNATECH
ELISPOT reader	C.T.L. ImmunoSpot Analyzer	Cellular Technology
Flow bench	HERA safe	Heraeus
Flow cytometre	MACS Quant analyzer	Miltenyi Biotec
Freezer (-20℃)/Fridge (4℃)	TKF380	EUREKA
Freezer (-80℃)	Hera Freeze	Heraeus
Gel chamber 40	1214 peqLab	PEQLAB
Gradient cycler	Px2 Thermal Cycler	Thermo
Hot plate	nuova II	Thermolyne
Incubator	HERA cell	Heraeus
Lab balance		Sartorius
Light Cycler	LightCycler 1.5	Roche

Magnetic stirrer	Magnetmix 2070	Hecht-Assistant
Micrometer	no. 7326	Mitutoyo
Microscope	Axioskop and Axioplan2	Carl Zeiss
Microscope camera	Axio Cam HRc	Carl Zeiss
Pipets	10µl, 100µl, 200µl, 1000µl; multichannel, multistepper	Eppendorf,
Pipettors	Pipetus	Hirschmann Laborgeräte
pH electrode	NEOLAB	Heidelberg
pH-metre	MV 870 Digital	PRÄCITRONIC
Power Supply	PowerPac300	Bio-Rad
Rotator	Coulter Mixer	Denleytech
Shaker	IKA-VIBRAX-VXR	IKA
Sonicator		Bandelin
Spectrophotometre	ND-1000	NanoDrop
Vortex	REAX 2000	Heidolph
Water bath	GFL1092	JULABO

5.6. Software

Software	Manufacturer
Axio Vision LE Application 4.5.0.0	Carl Zeiss
FlowJo 7.6.1	Tree Star, Inc.
GraphPad Prism 5	GraphPad Software
ImmunoSpot software 4.0.13	C.T.L. Cellular Technology
Light Cycler Software Version 3	Roche
MACSQuantify	Miltenyi Biotec
MetaVue	Molecular Devices
Revelation G3.2	Dynex

6. METHODS

6.1. Cell preparation and cell culture

6.1.1. Human B cells

Peripheral mononuclear cells (PBMCs) were isolated from blood filters from the blood donation of the Charité by densitiy gradient centrifugation using ficoll hypaque isolation (d = 1.007 g/ml) at 900 g, 30 min, room temperature. For magnetic cell sorting (MACS) of B cells, 2-5x10^8 PBMCs were labeled with 80 µl anti-CD19-coupled magnetic beads in a total volume of 400 µl MACS-buffer containing 40 µl beriglobin for blocking of unspecific bindings. After incubation for 15 min at 4℃ cells were washed with MACS-buffer and separated over a preequilibrated LS-column. The column was washed three times with 3 ml of MACS-buffer before B cells were eluted in 10 ml MACS-buffer. The purity of the cell population was ≥ 98% as assessed by flow cytometry and staining for CD19, CD14 for monocytes and CD3 for T cells. Cell count measurements of single cell solutions were performed with a CASY® cell counter.

6.1.2. Human naïve B cells

Human naïve ($CD19^+$ $CD27^-$)[65] B cells were isolated from PBMCs by MACS using anti-CD19 multisort beads. Cells were labeled and isolated as described in 6.1.1. $CD19^+$ B cells were incubated with 50 µl release solution in a total volume of 1 ml MACS-buffer for 10 min at 4℃ to remove magnetically coupled anti-CD19 beads. Subsequently B cells were labeled with anti-CD27 and anti-CD14 beads and separated over a LS-column. The negative fraction contained $CD19^+$ $CD27^-$ human naïve B cells. Purity was ≥ 98% for CD19 and ≥ 95% for CD27 as assessed by flow cytometry following staining for CD19, CD27 and CD14.

6.1.3. Cell culture conditions

All cell cultures were carried out at 37℃ and 5% CO_2 in a humidified atmosphere. Cells were cultivated at $1x10^6$/ml in Advanced RPMI / 5% CCS / 4mM L-glutamine / 100 U/ml penicillin / 100 µg/ml streptomycin. Charcoal-stripped FCS (CCS) was use to exclude the presence of VD_3 and $25(OH)VD_3$ in the medium.

6.2. Molecular biological methods

For gene expression analyses, $5x10^5$ naïve B cells were stimulated with 1 µg/ml anti-CD40 and 10 ng/ml recombinant human interleukin-4 (rh IL-4) for VDR-expression ± 100 nM calcitriol for 24 h. Afterwards RNA was isolated and transcribed into complementary DNA (cDNA), which was analyzed by quantitative PCR (qPCR).

6.2.1. RNA isolation

After stimulation, RNA was isolated using the Nucleospin®RNA II-kit according to the manufacturer´s guidelines. Briefly, cells were lysed in 350 µl RA1 lysis buffer containg 1% β-mercaptoethanol. Viscosity of lysates was reduced in a filter column, subsequently nucleic acids were bound to a silica membrane. Contaminating DNA was degraded by DNAse treatment directly on the column. After several washing steps, pure RNA was eluted with nuclease free water.
RNA concentration was measured photometrically at 260 nm using a ND-100 spectrophotometer.

6.2.2. cDNA synthesis

Complementary DNA (cDNA) synthesis was performed with Taq Man Reverse Transcription Reagent according to the manufacturer´s instructions. By combining oligo-dT primer and random hexamers cDNA synthesis was performed with Moloney Murine Leukemia Virus Reverse Transcriptase (RT). The cDNA mix contained the following ingredients:

	volume	***final concentration***
10x TaqMan RT buffer	2 µl	1x
25 mM $MgCl_2$	4.4 µl	5.5 mM
10 µM deoxyNTPs	4 µl	2 µM
50 µM random hexamers	0.5 µl	1.25 µM
50 µM oligo $d(T)_{16}$ primer	0.5 µl	1.25 µM
20 U/µl RNase inhibitor	0.4 µl	0.4 U/µl
50 U/µl MultiScribe RT	0.5 µl	1.25 U/µl
1 µg RNA		
dH_2O	ad 20 µl	

The following program was used in a thermal cycler:

25℃	10 min	primer binding
48℃	40 min	RT reaction
95℃	5 min	enzyme inactivation

6.2.3. Quantitative PCR

Quantitative PCR was performed in a Light Cycler 1.5 with the help of SYBR Green for quantification. SYBR Green is a cyanine dye that preferentially binds to double-stranded (ds) DNA. The DNA-dye-complex emits green light (522 nm) upon excitation with 488 nm. Therefore, fluorescence intensity increases when PCR products accumulate. Real-time PCR monitors the fluorescence emitted during the reaction as an indicator of amplicon production during each PCR cycle. Melting curve analysis was used to identify the specific amplicon and to exclude non-specific amplifications. For the reactions PCR LightCycler-Fast Start *Master* SYBR Green I was used according to manufacturers' guidelines. The reaction volume was reduced to 5 µl per sample. All samples were measured in duplicates. Water was used as a negative control. Primers were designed with the help of the online software Primer3 (http://frodo.wi.mit.edu/cgibin/primer3/primer3_www.cgi) and sequences are shown in Table 1. For every primer pair the optimal annealing temperature and $MgCl_2$ concentration as well as the efficiency were determined. In order to measure the relative expression levels, target genes were normalized to the expression of a

housekeeping gene, hypoxanthine guanine phosphoribosyltransferase (*hprt*). *hprt* expression is stable in the chosen experimental conditions. For analysis, the comparative c_p method was used according to the following formula:

$$R = \frac{(E_{target})^{\Delta c_p target(control-sample)}}{(E_{reference})^{\Delta c_p reference(control-sample)}}$$

Gene	***5' – 3' sequence***	***annealing temp***	***$MgCl_2$ [mM]***	***E***
HPRT for	TggCTTATATCCAACACTTCgTg	65℃	4	2.0
HPRT rev	ATCAgACTgAAgAgCTATTgTAATgACCA			
p105 for	CCAgTgAAgACCTCTCA	65℃	3	1.94
p105 rev	TgAgTTTgCggAAggATgTC			
cyp24 for	CgggTgTACCATTTACAACTCgg	65℃	5	1.88
cyp24 rev	CTCAACAggCTCATTgTCTgTgg			
vdr for	ACTTgCATgAggAggAgCAT	65℃	5	1.84
vdr rev	AggTCggCTAgCTTCTggAT			
p105 prom for	TggACCgCATgACTCTATCA	65℃	5	1.86
p105 prom rev	ggCTCTggCTTCCTAgCAg			
IκBα prom for	gACgACCCCAATTCAAATCg	60℃	3	1.8
IκBα prom rev	TCAggCTCggggAATTTCC			
Trpv6 ORF for	TgATgTCCAggCCCTgAACAAgT	60℃	5	2.0
Trpv6 ORF rev	gCTCCggggCAgCCTCCATCAgC			

Table 1: Primer sequences used for qRT-PCR (HPRT, p105, cyp24 and vdr for relative mRNA expression, p105 prom, IκBα prom and Trpv6 ORF for relative quantification of ChIP DNA). prom: promoter, E: efficiency

In case of ChIP analyses, DNA samples were quantified (see section 6.3.3), input DNA served as an internal control for normalization and the following formula was used:

$$R = E^{c_p\, input - c_p\, precipitated\, DNA}$$

I thank Dr. Guido Heine and Björn Hartmann for *cyp24* and *vdr* expression analyses in naïve and memory B cells.

6.3. Immunological methods

6.3.1. Western blot

Whole cell extracts were prepared with 1 ml Triton lysis buffer per $2x10^7$cells. Cytosolic and nuclear extracts were prepared with NE-Per extraction reagent.
Proteins were separated by gel electrophoresis. Gels consisted of a stacking gel (6% tris glycine sodium dodecyl sulfate polyacrylamide gel) and a resolving gel (12 % tris glycine sodium dodecyl sulfate polyacrylamide gel). Proteins were transferred to a polyvinylidenfluorid (PVDF) membrane and unspecific bindings were blocked with 5% milk powder/PBS for 1 h at room temperature. Membranes were incubated with primary antibodies for p50 or p65 in 1% milk powder/PBS-Tween (PBST) overnight at 4℃, washed 4 times in PBST and incubated with horseradish peroxidase (HRP)-coupled secondary antibodies in 1% milk powder/PBST 1 h at room temperature. After washing the membrane again, antigen detection was performed using the chemiluminescent ECL plus detection reagent. This solution contains the HRP-substrate luminol. The peroxidase and H_2O_2 catalyze the oxidation of luminol, so that light is emitted that causes signals on a radiographic film.

6.3.2. Co-Immunoprecipitation

With this technique it is possible to detect protein-protein interactions. One protein of interest is precipitated from a native cell lysate using a specific antibody. Subsequently the precipitated sample is subjected to western blot analysis, where interacting proteins can be detected.

Human naïve B cells were stimulated for 24 h with IL-4 to induce VDR-expression. Cells were than stimulated with calcitriol for 1 h or the complete culture period. Whole cell extracts were prepared using 1 ml Triton lysis buffer for $2x10^7$ B cells. Protein concentrations were determined with coomassie plus protein assay and 500 µg lysate were incubated with 2 µg rabbit anti-VDR antibody. As a control in one sample the antibody was preincubated with 5-fold excess of immunizing peptide, so that VDR cannot be precipitated in this sample. Magnetically coupled Protein A was added to the sample which was then separated in a magnetic field over an M-column. After extensive washing with Triton lysis buffer, VDR and interacting proteins were eluted from the column with 95℃ western blot sample buffe r and further analyzed by western blot.

6.3.3. Chromatin-Immunoprecipitation (ChIP)

Chromatin-Immunoprecipitation (ChIP) is a method to analyze the binding of transcription factors to promoter regions[66]. Formaldehyde fixed cells are lyzed and the DNA is sheared to pieces within a definded length by sonication. After immunonoprecipitation with an antibody of interest, the DNA that is pulled down is subjected to qPCR to delineate transcription factor binding under certain conditions.
To assess the influence of calcitriol mediated VDR activation on the binding of p65 to the p105 promoter, naïve B cells were stimulated with IL-4 for 24 h. Nuclear translocation of p65 and its binding to the p105 promoter were stimulated with anti-CD40 for 90 min with or without 1 h prestimulation with 1 µM calcitriol. Cells were harvested, washed in PBS and fixed with 1% formaldehyde for 10 min at room temperature. After addition of 0.125 M glycine for another 5 min, cells were pelletted at 350 g and lysed in 50 µl SDS lysis buffer. Cell lysates were diluted with 150 µl ChIP dilution buffer and the chromatin was sheared to 100-500 bp of length by sonication with 5 pulses of 10 s at 30% power. 300 µl of ChIP dilution buffer was added and the sample was precleared by adding 9 µl Protein A-coupled magnetic microbeads and 1µl salmon sperm DNA for 30 min at 4℃ and subjecting it to a µMACS column. The flow-through was further used as the precleared sample and 25 µl were kept as input. Immunoprecipitation was performed with 1 µg rabbit anti-p65 over night at 4℃. 45 µl Protein A-coupled magnetic microbeads and 5 µl salmon sperm DNA were added for 1 h. The antibody-bound fraction was separated in a

magnetic field using µMACS columns. The sample was diluted with 4% milk powder in ChIP dilution buffer and added to the column, which was washed 4 times with highsalt buffer, lowsalt buffer, LiCl and TE buffer. The ChIP fraction was eluted with 5 x 50 µl 65℃ ChIP elution buffer. Cross links were reversed by incubation at 65℃ over night in the presence of 200 mM NaCl.
DNA extraction of ChIP samples and input fractions was done with the NucleoSpin Extract II Kit following the manufacturer´s instructions and using NTB buffer for samples containing SDS.

6.3.4. Flow Cytometry

By means of flow cytometry single cells can be analyzed due to their light scatter characteristics and their differential expression of surface or intracellular markers, which are stained with fluorochrome-labeled antibodies. At first, different cell populations can be roughly distinguished with the help of forward light scatter (FSC) and side light scatter (SSC) according to their size and granularity, respectively. Additionally, fluorochrome-labeled markers are excited by different lasers and the emitted light is detected by different photomultiplier tubes (PMT). The specificity of detection is controlled by optical filters. Band bass filters transmit light within a certain range of wavelengths, long pass filters transmit light above a certain wavelength.
Single and multicolor stainings were analyzed on a MACSQuant® Analyzer equipped with a violet laser (405 nm), a blue argon laser (488 nm) and a red laser (635 nm).

6.3.4.1. Flow cytometric analysis of IκBα degradation

$CD19^+$ B cells were stimulated with rhIL-4 for 24 h. NF-κB activation and subsequent IκBα degradation was induced with anti-CD40 for 15, 30 and 45 min. To assess the effect of calcitriol on IκBα degradation cells were pretreated with 100 nM calcitriol for 1 h before anti-CD40 stimulation. Cells were fixed with 2% paraformaldehyde (PFA) for 10 min at 37℃, washed in FACS buffer and stained with anti-CD27 (LG.7F9) for 15 min at 4℃. After an additional washing step, cells were stained with anti-IκBα (L35A5) in 1 % saponin / FACS buffer for 30 min at 4℃. Cells were immediately analyzed at the flow cytometer. At least 30000 gated B cells were collected for each sample and geometric mean fluorescence intensity was analyzed.

6.3.4.2. Flow cytometric analysis of murine splenic B and T cell composition

To analyze the B and T cell composition in spleens of CYP27$^{-/-}$ mice and wt controls, 2x10^6 splenocytes were stained for each panel. At first unspecific bindings were blocked with anti Fcγ-receptor (2.4G). For the T cell panel cells were stained with CD3ε (145-2C11), CD4 (GK1.5), CD8 (53-.7), CD62L(MEL14) and CD44 (IM7) for 15 min on ice. Cells were gated in CD3$^+$ CD4$^+$ or CD3$^+$ CD8$^+$ and these subsets were analyzed for their expression of CD62L and CD44 to differentiate between naïve and memory T cells. The CD44 staining was controlled with an isotype control. For the B cell panel cells were stained with CD19 (1D3), CD21 (7G6) and CD23 (B3B4). CD19$^+$ cells were analyzed for their expression of CD21 and CD23 to differentiate between follicular (FO, CD21$^+$, CD23$^+$) and marginal zone (MZ, CD21^{high}, CD23$^-$) B cells[67]. 15000 cells were collected in the CD3 gate and the CD19 gate, respectively.

6.3.4.3. Flow cytometric analysis of OVA specific plasma cells

To analyze OVA specific IgG1$^+$ plasma cells 2x10^7 splenocytes were used for each staining. At first unspecific bindings were blocked with anti Fcγ-receptor (2.4G) and the cell surface was stained with anti-B220 (RA3.6B2), anti-CD138 (281-2) and anti CD38 (clone 90) in the presence of 7 aminoactinomycin D (7-AAD) for dead cell exclusion. After washing, cells were fixed with 2% PFA for 10 min at 4℃. Cells were washed in 0.5% saponin/FACS buffer and stained intracellularly with anti-IgG1 (X56) and OVA in 0.5% saponin/FACS buffer for 30 min at 4℃. As a control, one sample was blocked with 1000 fold excess of unlabeled OVA. After a final washing step cells were analyzed at the flow cytometer and the maximum cell number was collected. OVA specific IgG1$^+$ plasma cells were defined as 7-AAD$^-$, CD138$^+$, B220^{low}, IgG1^{high} and OVA$^+$.

6.3.4.4. Flow cytometric analysis of T regulatory cells

Regulatory T cells were stained using the Mouse Regulatory T cell Staining Kit 3 following the manufacturer´s protocol. All incubation steps were carried out at 4℃. Briefly, 1x10^7 cells were washed with PBS/1% BSA and unspecific bindings were blocked with anti Fcγ-receptor (2.4G) for 15 min. The cell surface was stained with anti-CD4 (RM4-5) and anti-CD25 (PC61.5) for 30 min. After washing, 1 ml of freshly

prepared Fixation/Permeabilization working solution was added to each sample for 18 h. Cells were washed twice in Permeabilization Buffer, blocked with 50 µl Fc block (CD16/32) for 15 min and stained intracellularly with anti FoxP3 (FJK-16s) for 30 min. Cells were washed twice in Permeabilization Buffer and resuspended in FACS buffer for flow cytometric analysis.

6.3.5. Enzyme-linked immunosorbent assay (ELISA)

6.3.5.1. Immunoglobulin ELISA

ELISA	*coating antibody*	*blocking reagent*	*standard*	*secondary antibody*
IgE	rat anti-mouse IgE R35-72, BD	PBS/3% milk	mouse IgE, κ BD	anti-IgE-Bio EM 95.3, DRFZ
IgG1	goat anti-mouse IgG1 1070-01 Southern Biotech	PBS/3% BSA	mouse IgG1, κ BD	anti-IgG-AP 1030-04 Southern Biotech
IgA	goat anti-mouse IgA 1040-01 Southern Biotech	PBS/3% BSA	mouse IgA, κ S107 Southern Biot	anti-IgA-AP 1040-04 Southern Biotech
IgG2c	goat anti-mouse IgG2c Bethyl	PBS/3% BSA	mouse IgG2c reference serum	anti-IgG2c-HRP Bethyl
IgM	goat anti-mouse IgM 1020-01 Southern Biotech	PBS/3% BSA	mouse IgM PP50, Chemicon	anti-IgM-AP 1020-04 Southern Biotech

Table 2: Antibodies and reagents used for total immunoglobulin ELISAs

ELISA was used to quantify serum immunoglobulin concentrations of total and OVA-specific IgE, IgG1 and IgA. Maxisorp plates were coated with the primary antibody or OVA in sodium carbonate buffer overnight at 4℃. Plates were blocked for 2 h at room temperature and sera were added in appropriate serial dilutions for 2 h. After washing with PBS/0.5% Tween secondary antibodies were added. In case of all OVA-specific ELISAs and total-IgE, biotinylated secondary antibodies were used. Therefore, SA-HRP was added and TMB was used as a substrate. The use of AP required pNPP as a substrate. Details about antibodies and blocking reagents can be found in Table 2 for total immunoglobulins and in Table 3 for OVA-specific immunoglobulins.

ELISA	***coating antibody***	***blocking reagent***	***standard***	***secondary antibody***
IgE	rat anti-mouse IgE R35-72, BD	PBS/3% BSA	serum pool	OVA-Bio DRFZ
IgG1	OVA	PBS/3% milk	OVA 14 IgG1 Sigma	anti-IgG1-Bio A85, BD
IgA	OVA	PBS/3% milk	serum pool	anti-IgA-Bio 1040-08 SouthernBiotech
IgG2c	OVA	PBS/3% BSA	serum pool	anti-IgG2c-HRP Bethyl
IgM	OVA	PBS/3% BSA	serum pool	anti-IgM-AP 1020-04 SouthernBiotech

Table 3: Antibodies and reagents used for OVA-specific immunoglobulin ELISAs

6.3.5.2. 25(OH)VD_3 ELISA

Serum concentrations of 25(OH)VD_3 in mice were determined with the 25-Hydroxy Vitamin D EIA from immunodiagnostiksystems following the manufacturer´s instructions.

6.3.6. Enzyme-linked immunospot assay (ELISPOT)

The ELISPOT assay is used to detect single antibody-secreting cells[68]. Multiscreen $_{HTS}$-IP 96 well plates with PVDF membranes were prewetted with ethanol and coated with 100 µl 100µg/ml OVA in sodium carbonate buffer overnight at 4℃. Wells were blocked with RPMI-1640/10% FCS and PBS/3% BSA (1:1 dilution) for 1 h at 37℃, 5% CO_2. Single cell suspensions of spleen and bone marrow were resuspended in RPMI-1640/10% FCS. For IgG1 $2.5x10^6$ cells and for IgA $5x10^6$ cells were seeded into the first row and three-fold serial dilutions were performed and incubated in the plates overnight at 37℃, 5% CO_2. After extensive washing with PBS/0.05% Tween 20 biotinylated detection antibodies were incubated for 4 h at room temperature (IgG1 A85.1; IgA 1040-08). Plates were washed again and incubated with SA-HRP for 1 h at room temperature. Spots were visualized with 100 µl/well AEC substrate solution and counted with a C.T.L. ImmunoSpot Analyzer and ImmunoSpot software 4.

6.3.7. Frozen sections of mouse spleens

Approximately 25% of each spleen was cut out of the middle and embedded in freezing medium and carefully frozen on dry ice. The tissue was cut into 7 µm specimens with a microtome at -18℃ and directly transferred to Superfrost microscope slides. The slides were dried at 50℃ and fixed in acetone. After drying, slides were stored with calcium chloride at -80℃ until further analysis.

6.3.8. Immunohistology

Sections were rinsed with PBS and endogenous peroxidases were blocked with 0.3% H_2O_2 in methanol for 20 min. After washing 3 times with PBS/0.05% Tween sections were blocked with avidin/biotin blocking solution and, subsequently, with PBS/3% BSA for 30 min. Sections were incubated with FITC-coupled anti-B220 and biotinylated anti-MOMA-1 for 1 h. Afterwards, slides were stained with anti-FITC-HRP, wshed again and developed with the NovaRed substrate kit following the manufacturer´s instructions. After incubation with SA-AP, development with the NovaBlue substrate kit was performed. Sections were rinsed under running tap

water, mounted and coverslipped. Slides were analyzed in a bright-field microscope and the Axio Vision software.

6.4. Animal work

6.4.1. Breeding of mice

CYP27B1$^{-/-}$ mice were provided by Professor René St-Arnaud[69]. They lack exon 8 of CYP27B1 containing the heme binding domain. Mice were bred and maintained under specific pathogen free conditions in the animal facility of the Charité. The experiments were conducted according to the German animal protection law.

6.4.2. Genotyping of CYP27B1$^{-/-}$ mice

5 mm tail biopsies were lysed and genomic DNA was isolated using the NucleoSpin Tissue Kit according to the manufacurer´s instructions. PCRs were performed on tail DNAs to determine the genotype. The use of the primer pair CYP27 gen for (CCTgTTCCCTCAggTATCCA) and CYP27 gen rev (CCTggCTCAggTAgCACTTC) resulted in a ~1400 bp band in wt mice and in a ~800 bp and in ko mice. PCR mix contained the following ingredients:

	volume	***final concentration***
10x GenTherm buffer	2.5 µl	1x
50 mM $MgCl_2$	1.25 µl	2.5 mM
10 mM deoxyNTPs	0.25 µl	100 nM
10 µM forward primer	0.5 µl	200 nM
10 µM reverse primer	0.5 µl	200 nM
5 U/µl DNA polymerase	0.25 µl	0.05 U/µl
DNA	1 µl	
dH_2O	ad 25 µl	

The following PCR program was used:

95 ℃	2 min	
94 ℃	20 sec	40 cycles
65 ℃	30 sec	
72 ℃	1 min	
72 ℃	10 min	
4 ℃	forever	

2.5 µl of 10x DNA loading buffer were added to 25 µl PCR products and separated on a 1% agarose gel. Gels were photographed with a UV light photometer and bands were analyzed to determine the genotype. DNA of wt mice showed a 1400 bp band, DNA of ko mice showed a 800 bp band, both bands are present in DNA of heterozygous mice.

6.4.3. Diets

CYP27B1$^{-/-}$ mice suffer from pseudovitamin D-deficiency rickets (PDDR)[69]. To prevent this, ko mice were fed with a high calcium rescue diet containing 2% calcium, 1.25% phosphorus and 20% lactose[70]. One group of wt received the same diet. A second group of mice received a standard chow containing 1% calcium, 0.7% phosphorus, 0% lactose and 1 kIU/kg Vitamin D_3.

6.4.4. Type-I sensitization

Mice were sensitized intraperitoneally (i.p.) with 100 µl of 10 µg ovalbumin (OVA) adsorbed to 1.5 mg $Al(OH)_3$ (alum) on days 1, 14 and 21. To enhance the IgE immune response, which is quite low in C57Bl/6 mice, mice were boosted on day 50.

6.4.5. Allergen-induced cutaneous hypersensitivity reaction

A cutaneous hypersensitivity reaction was induced with allergen as a functional assay to investigate the influence of the lack of endogenous CYP27B1 in a mast cell

and IgE and IgG1 dependent reaction. Mice were anaesthetized with an i.p. injection of Ketamin / Rompun (5 mg/ml Ketamin, 0.2% Rompun in 0.9% NaCl).The dose was adapted to the body weight. 100 µg OVA dissolved in 20 µl PBS were injected into one earlobe intradermally. 20 µl PBS were injected into the other ear as a control. Ear thickness was measured before OVA application and 2 h afterwards with a micrometer (Mitutoyo no. 7326).

6.4.6. Blood samples

Blood samples were taken from the *vena facialis* by punctuating it with a microlancet. The blood was directly collected into serum separator tubes and centrifuged at 6800 g for 10 min. Serum was stored at -80℃ until further analysis.

6.4.7. Organ preparation

6.4.7.1. Spleen

Freshly removed organs were place in 1.5 ml PBS/EDTA on ice. Approximately 75% of the spleen was used for lymphocyte analysis. The organs were weighed in order to calculate the cell numbers of the whole spleens. Spleens were pressed through 100 µm filters with plungers of 5 ml syringes. The suspension was filtered again with a 40 µm filter in PBS/EDTA. After pelletting the cells, erythrocytes were removed by incubation with 2.5 ml RBC lysis buffer for 5 min on ice. 30 ml PBS/EDTA were added and the cells were centrifuged again. Cells were passed through a preseparation filter to remove residual cell aggregates, counted and resuspended in RPMI/10%FCS. Spleens were weight before and after removing a piece for histology, so that total cell numbers could be calculated.

6.4.7.2. Bone marrow

Tibia and femur of dissected mice were cut and flushed with PBS/EDTA. Preparation of single cell suspensions was done as for spleens. Tibia and femur contain 18.7% of total bone marrow, so that cellc numbers were multiplied with the factor 5.3 to receive total bone marrow cell numbers[71].

6.5. Statistics

Statistical analyses were performed using Graph Pad Prism 5 Software. To analyze paired data sets, Wilcoxon signed test for non-parametrical, paired data was used. Unpaired data sets were analyzed with the Mann-Whitney U-test. In case of normal distribution a non-paired t-test was used. A p-value ≤ 0.05 was considered to be statistically significant.

7. RESULTS

7.1. Calcitriol impairs NF-κB activation in human naïve B cells

7.1.1. Activated vitamin D receptors inhibit p105 expression in human naïve B cells

To investigate the role of the VDR in the regulation of NF-κB p105 and p50 in B cells, at first the B cell target population of the natural VDR agonist calcitriol was identified. Naïve ($CD27^-$) and memory ($CD27^+$) B cells were distinguished according to their CD27 surface expression[72]. Among these cells expression of *vdr* and its target gene[73] *cyp24a1* were investigated after stimulation with anti-CD40, IL-4 and calcitriol. In naïve B cells, *vdr* expression was 2.8 to 4-fold higher than in memory B cells. Furthermore, the VDR target-gene *cyp24a1* was induced 4.3 to 8.2-fold stronger in naïve than in memory B cells (**Table 4**). Thus, all following experiments were carried out with naïve $CD19^+$ $CD27^-$ B cells.

To elucidate the impact of calcitriol on p105 expression, qRT-PCR was performed with RNA isolated from naïve B cells. Stimulation with anti-CD40 and IL-4 increased p105 expression by 56 ± 5% (p=0.008) compared to unstimulated B cells and calcitriol reduced p105 expression to 72 ± 5% (p=0.003) of the stimulated control (Figure 5A). Additionally, it was investigated, whether this transcriptional inhibition of p105 mRNA expression resulted in a reduced protein amount of NF-κB p105 and p50. Protein expression was induced by stimulation with anti-CD40 and IL-4. Additional incubation with calcitriol resulted in a substantial reduction of NF-κB p50 and also p105 protein expression. In contrast, NF-κB p65 remained stable by anti-CD40 and IL-4 stimulation, also if calcitriol was added (Figure 5B). These data show that VDR activation results in impaired NF-κB p105 expression.

donor	*cyp24a1* induction naïve/memory	*vdr* induction naïve/memory
1	8.2	4
2	4.7	2.8
3	4.3	3.1

Table 4. Calcitriol acts predominantly in naive B cells. Naive (CD19+ CD27-) and memory (CD19+ CD27+) B cells were magnetically sorted and stimulated with anti-CD40 and IL-4 for 24 h. Expression of *vdr* and the VDR responder gene *cyp24a1* were analyzed by q-RT PCR upon calcitriol stimulation. Data of three individual donors are shown as ratios of mRNA induction of naïve to memory B cells.

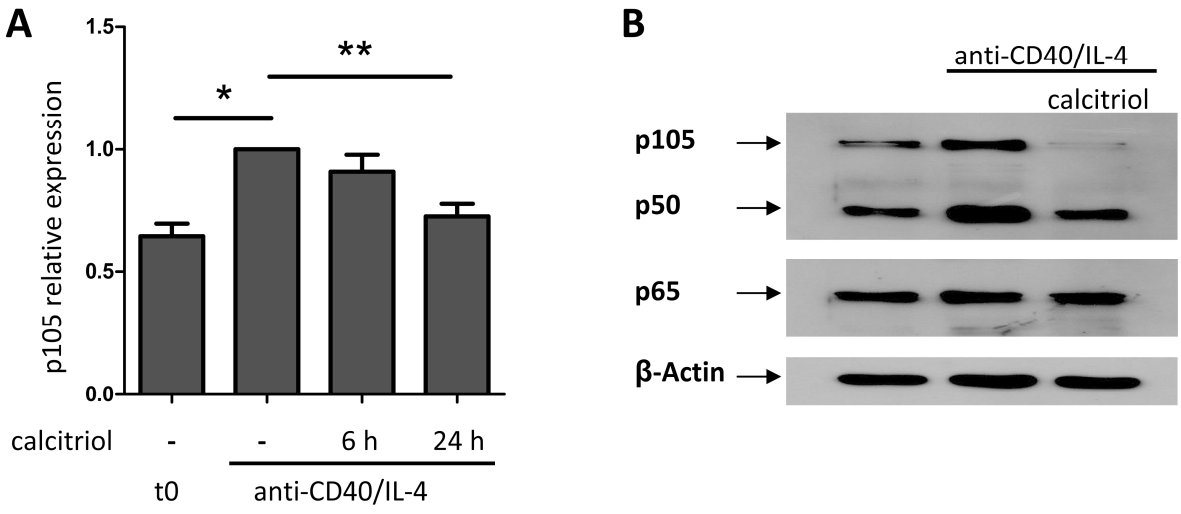

Figure 5. VDR ligation reduces p105 transcription and protein expression in human naive B cells. Naive B cells were magnetically sorted as $CD19^+$ $CD27^-$. Cells were stimulated for 24 h with anti-CD40 and IL-4 in the presence or absence of 100 nM calcitriol. **A** p105 mRNA expression was determined in relation to HPRT. n≥8. * p≤0.05, ** p≤0.005. t0: ex vivo**. B.** Whole cell extracts were subjected to western blot analysis for NF-κB p105/p50 and NF-κB p65. β-Actin was used as a loading control.

7.1.2. Reduced nuclear translocation of p65 upon vitamin D receptor activation

The major transcription factor inducing NF-κB p105 transcription is p65[74]. Therefore, in the next step the effect of calcitriol on p65 translocation was examined. To avoid NF-κB activation during the induction of VDR in naïve B cells, the cells were prestimulated with IL-4 only (24 h)[73, 75]. This procedure did not significantly activate NF-κB as shown by low nuclear p65 amounts (Figure 6). Accordingly, nuclear translocation of p65 was induced after stimulation with anti-CD40 (1 h). The impact of VDR ligation was assessed by addition of calcitriol to the cells (1 h) prior to CD40 activation. The data show that in the presence of calcitriol a considerably diminished p65 nuclear translocation occured (Figure 6).

Generally, p65 is retained in the cytosol by the IκB-family. Among these IκBα has the highest affinity to p65[52]. Upon stimulation with anti-CD40, IκBα is phosphorylated by the IκB kinase complex and subsequently degraded by the proteasome. Thereby, p65 translocates into the nucleus. Herein, it was analyzed whether IκBα protein expression is altered or whether its degradation is inhibited by calcitriol (Figure 7). At first the specificity of the IκBα-staining was confirmed by blocking the staining with a blocking peptide (Figure 7A). The data show that in naive B cells IκBα protein expression is not enhanced upon calcitriol treatment (Figure 7B). Also anti-CD40 induced IκBα degradation is unchanged upon calcitriol stimulation (Figure 7C) and thus, p65 translocation is most likely reduced by an IκBα independent mechanism.

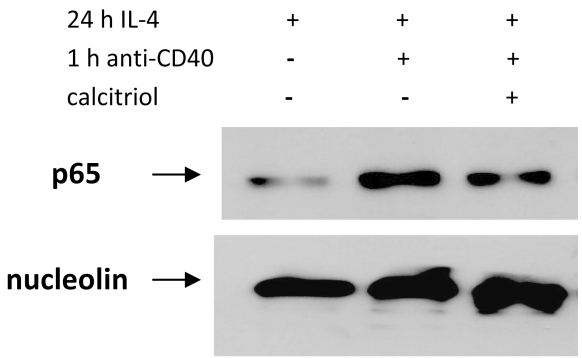

Figure 6. VDR ligation inhibits p65 activation in human naive B cells. Naive B cells were magnetically sorted as $CD19^+$ $CD27^-$. After 24 h stimulation with IL-4 alone nuclear translocation of p65 was induced with anti-CD40 for 1 h. Cells were prestimulated with 100 nM calcitriol for 1 h and nuclear extracts were analyzed by western blot for p65. Nucleolin was used as a loading control.

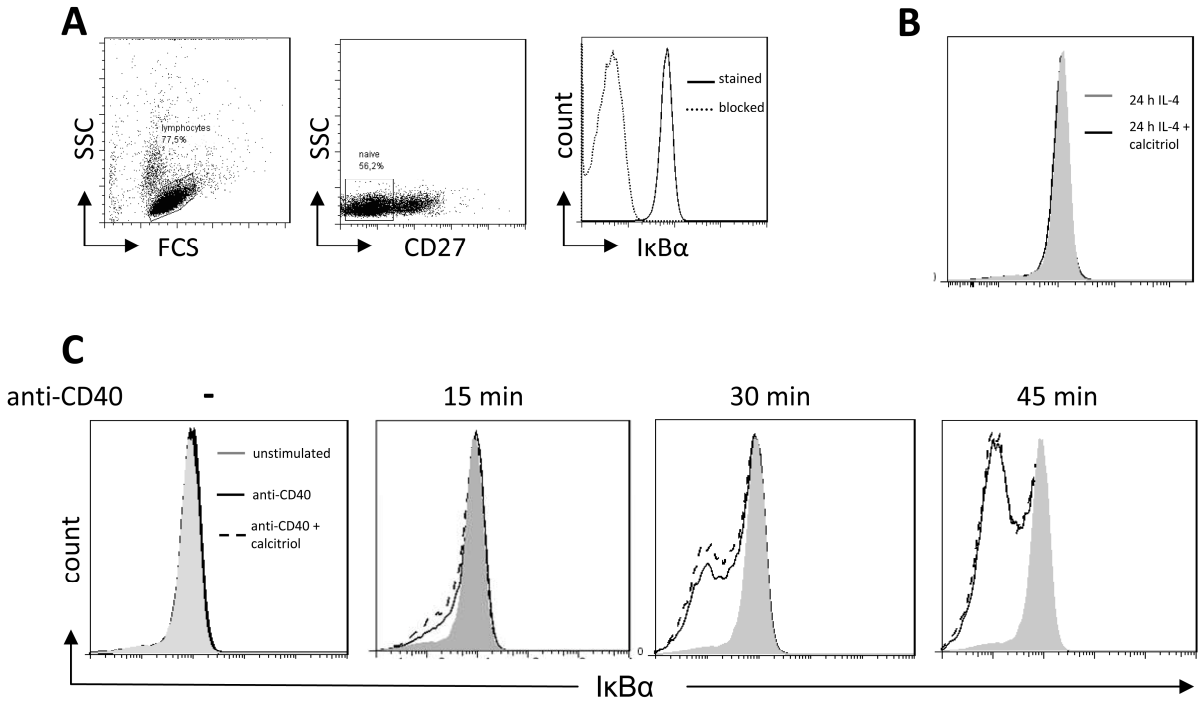

Figure 7. IκBα degradation remains stable upon calcitriol treatment. A. Naïve B cells were identified as $CD27^-$ lymphocytes. Preincubation of anti-IκBα with a blocking peptide proves the specificity of the staining. **B.** B cells were stimulated with IL-4 for 24 h with/out additional calcitriol (100 nM) to analyze the influence of calcitriol on IκBα protein expression. **C.** B cells were stimulated with IL-4 for 24 h. Cells were pretreated with 100 nM calcitriol for 1 h. IκBα degradation was induced by anti-CD40 stimulation for 15, 30 and 45 min, respectively. Degradation of IκBα was assessed by flow cytometry. Filled histograms: unstimulated cells, black lines: anti-CD40, dashed lines: anti-CD40 + calcitriol. One representative experiment out of four is shown.

7.1.3. Protein complexes between VDR and p65 are not detectable

As the retention of p65 in the cytosol is not due to alterations of IκBα protein expression or activity, it was next investigated whether VDR and p65 build protein complexes which may be a cause of cytosolic retention. After immunoprecipitation of the VDR, western blot analysis showed that both, VDR and p65 were expressed in IL-4 stimulated naïve B cells (Figure 8, input). After preincubating the anti-VDR antibody with its blocking peptide, precepitation of the VDR was completely blocked. The western blot for p65 showed prominent bands of approximately 50 kD representing the antibody heavy chains that are in the IP samples. Nevertheless, the 65 kD bands representing NF-κB should be clearly separated from the antibody heavy chains. No signal for p65 was obtained.

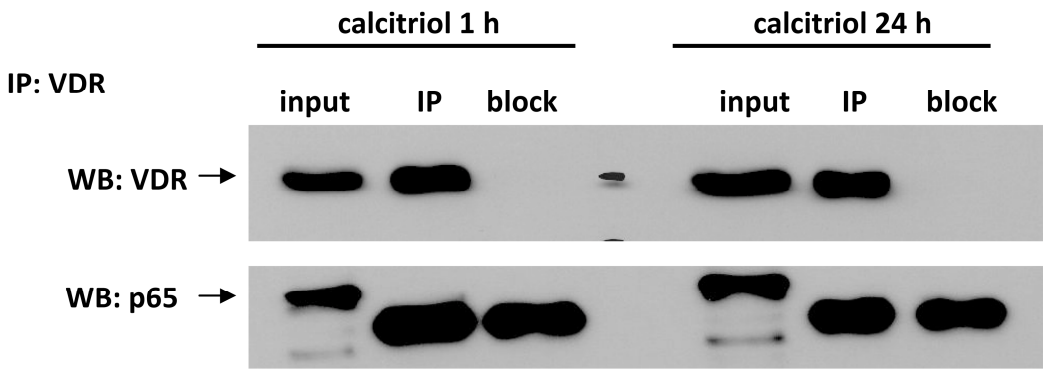

Figure 8. No protein complexes between VDR and p65 are detectable. Human naïve B cells ($CD27^-$) were stimulated for 24 h with IL-4 to induce VDR-expression. Cells were than stimulated with 100 nM calcitriol for 1 h or the complete culture period. Whole cell extracts were prepared using 1 ml Triton lysis buffer for $2x10^7$ B cells. Protein concentration was determined with coomassie plus protein assay and 500 µg lysate were incubated with 2 µg rabbit anti-VDR antibody. As a control in one sample the antibody was preincubated with 5-fold excess of immunizing peptide, so that VDR cannot be precipitated in this sample (block). Magnetically coupled ProteinA was added to the sample which was then separated in a magnetic field over an M-column. After extensive washing with Triton lysis buffer, VDR and interacting proteins were eluted from the column with 95°C western blot sample buffer and further analyzed by western blot. IP: immunoprecipitation; WB: western blot, input: unprecipitated DNA

7.1.4. Impaired binding of p65 to the p105 promoter by calcitriol

As NF-κB p65 is the main inducer of p105 transcription[74], it was investigated whether the inhibition of p65 nuclear translocation leads to an impaired binding of p65 on the p105 promoter using chromatin immunoprecipitation (ChIP). Naïve B cells were stimulated as described for the p65 translocation analyses. Following fixation, the cell lysates were sonicated and p65 immunoprecipitation was performed. Binding of p65 protein to the p105 promoter was analyzed by qPCR-amplification of the promoter region containing a kappa-B (κB) regulatory element. Amplification of the known p65 binding site in the IκBα promoter proofed that p65 was activated and bound to DNA after anti-CD40 stimulation (Figure 9). Anti-CD40 stimulation also resulted in p65 binding to the p105 promoter. Calcitriol stimulation reduced p65 binding to the p105 promoter back to baseline in unstimulated cells (Figure 9). Accordingly, in the negative control region in the *trpv6* ORF that contains no p65 binding site, no activation or calcitriol-regulated p65 signal was obtained (Figure 9).

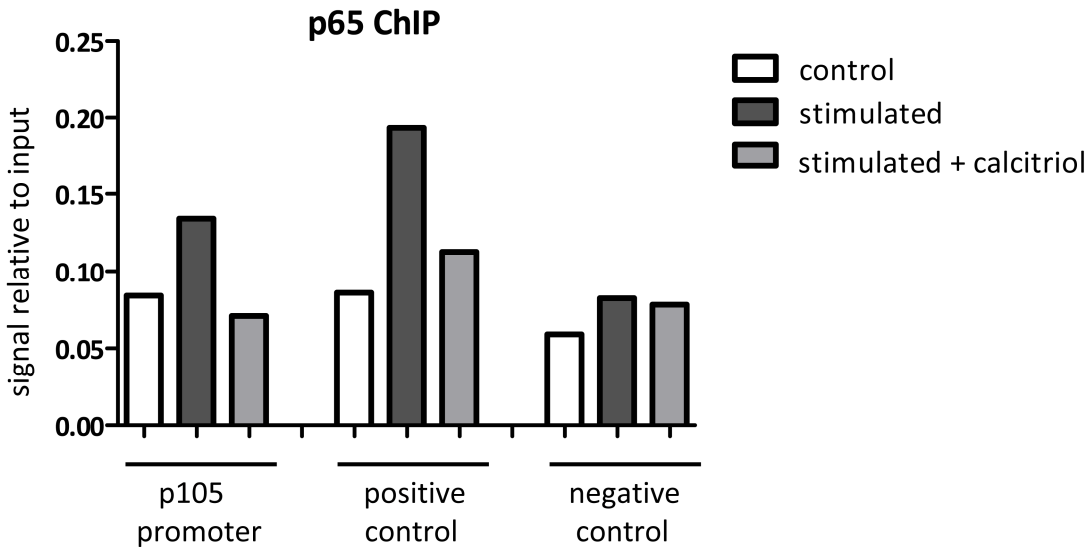

Figure 9. VDR activation impairs binding of p65 to the p105 promoter. Naive $CD27^-$ B cells were stimulated with IL-4 for 24 h. p65 was activated with anti-CD40 with/out 1 h prestimulation with 1 µM calcitriol and chromatin immunoprecipitation (ChIP) was performed with an anti-p65 antibody. p105 promoter, IκBα promoter (positive control for p65 binding) and trpv6 ORF (negative control) were amplified by qPCR. Signals are shown relative to input (unprecipitated) DNA. One representative experiment out of three is shown.

7.2. Targeted inactivation of CYP27B1 alters the humoral immune response

7.2.1. CYP27B1$^{-/-}$ mice were analyzed in a mouse model for allergic sensitization

The influence of endogenously produced calcitriol during the course of a type-I sensitization was analyzed in a mouse model using CYP27B1$^{-/-}$ mice which cannot produce calcitriol from the precursor 25(OH)VD_3. Their wt littermates were used as controls. Mice received a rescue diet containing defined amounts of calcium and phosphorus as well as 20% lactose to enable passive calcium resorption and to prevent mice from suffering from rickets and osteomalacia[70]. The rescue diet did not contain VD_3. One group of wt mice received the same diet as a control (wt 0 kU VD_3). These mice were VD deficient. The second group received a standard diet (wt 1 kU VD_3) providing an adequate amount of VD_3. Mice where fed with their special diets from 4 weeks of age for 7 to 9 weeks before the sensitization started and throughout the experiment. Mice were sensitized with OVA/alum at days 1, 14 and 21 and boosted at day 50. Blood samples were taken at days 0, 35, 56 and 100. Day 35 has been shown to present the peak of the OVA-specific IgE immune response after three i.p. injections of OVA/alum, while the OVA boost at day 50 is expected to induce maximum OVA-IgE concentrations within 5 to 7 days[76]. An ear swelling test was performed at day 99. Finally, mice were sacrificed at day 100 (Figure 10).

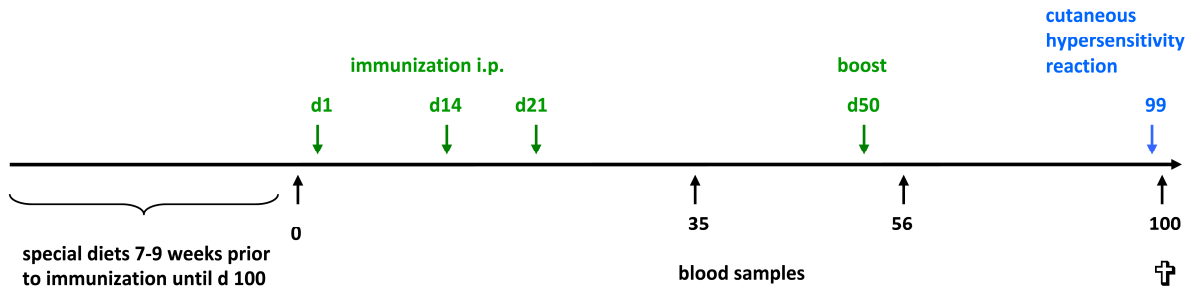

Figure 10. Experimental setting. Mice were sensitized i.p. with 10 µg OVA/alum at days 1, 14 and 21. An additional boost was performed at day 50. Blood samples were taken at days 0, 35, 56 and 100. A cutaneous hypersensitivity reaction was induced with OVA at day 99, mice were sacrificed at day 100.

7.2.2. CYP27B1$^{-/-}$ mice are VD deficient and have a reduced body weight

The body weight was assessed at day 1 of the experiment when mice were initially sensitized and throughout the experiment. CYP27B1$^{-/-}$ were smaller from the beginning (17.4 ± 0.6 g) and did not gain weight until day 100 (17.8 ± 0.9 g) (Figure 11A). Wt mice receiving a standard diet had a normal physiological body weight at day 1 (19.2 ± 0.4 g) and gained weight with age (21.7 ± 0.4 g). VD deficient wt mice, that received the 20% lactose containing diet, were taller (day 1: 21.7 ± 0.6 g; day 100: 23.5 ± 0.6 g) and in contrast to ko mice more subcutaneous fat was visible after scarification. Spleen and bone marrow cell numbers were counted after single cell isolation and erythrocyte lysis. Cell numbers did not significantly differ between the groups. However, CYP27B1$^{-/-}$ were smaller than wt spleens by tendency (Figure 11C, D). 25(OH)VD_3 serum concentrations were measured by ELISA at different time points. Since they did not change over time only day 0 is shown. CYP27B1$^{-/-}$ and VD deficient wt mice had significantly lower 25(OH)VD_3 serum concentrations (ko: 59.8 nM, [51.1 – 67.8 nM]; VD deficient wt: 60 nM, [45.3 – 116.1 nM]) than the wt controls receiving a normal amount VD_3 with the chow (94.2 nM, [70.5 – 169.2 nM]) (Figure 11B).

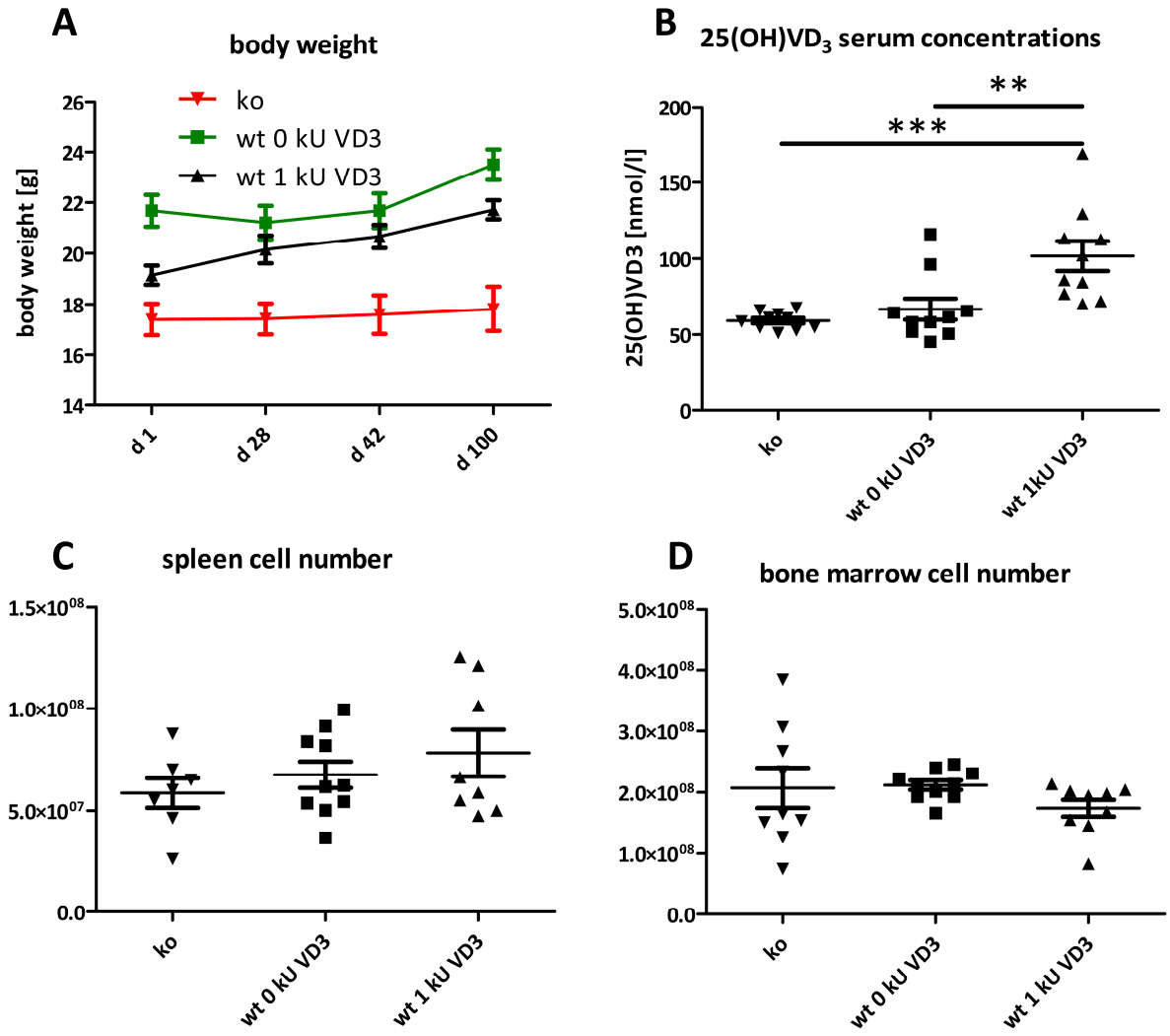

Figure 11. CYP27B1$^{-/-}$ mice are VD deficient and have a reduced body weight. A. Body weight was assessed from day 1, when mice received their first sensitization. **B.** 25(OH)VD_3 serum concentrations were measured by ELISA at day 0. 25(OH)VD_3 serum concentrations were stable throughout the experiment. **C, D.** Spleen and bone marrow cell numbers were counted at day 100 after single cell isolation and lysis of erythrocytes. Data are shown as single values and the medium for each group (n≥8). ** p≤0.005, *** p≤0.001.

7.2.3. Lack of endogenous calcitriol production alters the humoral immune response

The course of the humoral immune response was followed by taking blood samples at days 0, 35, 56 and 100. Serum concentrations of IgE, IgG1, IgA, IgG2c and IgM were measured by ELISA (Figure 12). IgE concentrations were 3-fold higher in CYP27B1$^{-/-}$ mice already at day 0 before the first sensitization (p=0.0052, Figure 12A). The difference was temporarily not present at day 56 shortly after the boost and

became again pronounced at day 100 (6-fold, p=0.019). Besides IgE, IgM was the only immunoglobulin with significantly higher serum concentrations in ko mice before (2.2-fold) and after sensitization (1.4-fold, Figure 12E). In both cases the two wt groups did not differ. The lowest IgG1 serum concentrations were found in the wt group receiving the standard chow with 1 kU VD3. In VD deficient wt mice and CYP27B1$^{-/-}$ 1.9 – 2.5-fold elevated levels of IgG1 were transiently observed at day 35 and 56, respectively, when the OVA triggered immune response was still ongoing (Figure 12B). At day 100 all groups had comparable IgG1 serum concentrations (ko vs wt: p=0.54; ko vs VD deficient: p=0.87). IgG2c concentrations were significantly reduced in VD deficient wt mice (1.8-fold) and CYP27B1$^{-/-}$ mice (1.9-fold) compared to the wt control mice only at day 100 (Figure 12D). Interestingly, IgA serum concentrations were significantly higher in CYP27B1$^{-/-}$ mice at days 35, 56 and 100, with more pronounced differences over time (Figure 12C). Only in ko mice IgA was strongly induced during the course of the experiment (ko day 0: 136.3 ± 19 ng/ml, day 100: 465.9 ± 68.4 mg/ml; wt day 0: 135 ± 33.6 mg/ml, day 100: 223.8 ± 79.7 mg/ml).

OVA-specific immunoglobulins were not detectable before OVA sensitization at day 0. All isotypes measured were significantly higher in CYP27B1$^{-/-}$ mice at day 100. The most striking difference was observed for OVA-IgA, with 7.8-fold higher concentrations in ko than in wt mice. OVA-IgE was elevated 4.8-fold and OVA-IgG1 3-fold in ko mice. The wt groups were comparable (Figure 13). OVA-IgM and OVA-IgG2 were only detected at day 100.

To analyze whether different immunoglobulin serum concentrations in CYP27B1$^{-/-}$ and wt mice go along with differences in the numbers of antibody secreting cells (ASC), ELISPOT was performed at day 100 of the experiment for spleen and bone marrow. Interestingly, IgG1 ASC were significantly higher in the spleen and significantly lower in the bone marrow of CYP27B1$^{-/-}$ mice compared to wt mice receiving a standard diet (Figure 14A, B). CYP27B1$^{-/-}$ mice had lower total numbers of OVA-IgG1 ASC as summed up from spleen and bone marrow (25576 [6783 – 42338] cells) than wt mice (43628 [23074 – 51565] cells). Results for VD deficient wt mice were subject to variation. The elevated number of OVA-IgG1 ASC could be confirmed by intracellular staining and FACS analysis of splenocytes (Figure 15B). OVA-IgG1 specific plasma blasts and plasma cells (ASC) were defined as B220^{low}, IgG1^{+}, CD138^{+} and OVA^{+}. The specificity of the OVA staining was confirmed by

successful blocking of the staining with 1000-fold excess of unstained OVA (1.6% versus 0.2% positive cells) (Figure 15A).

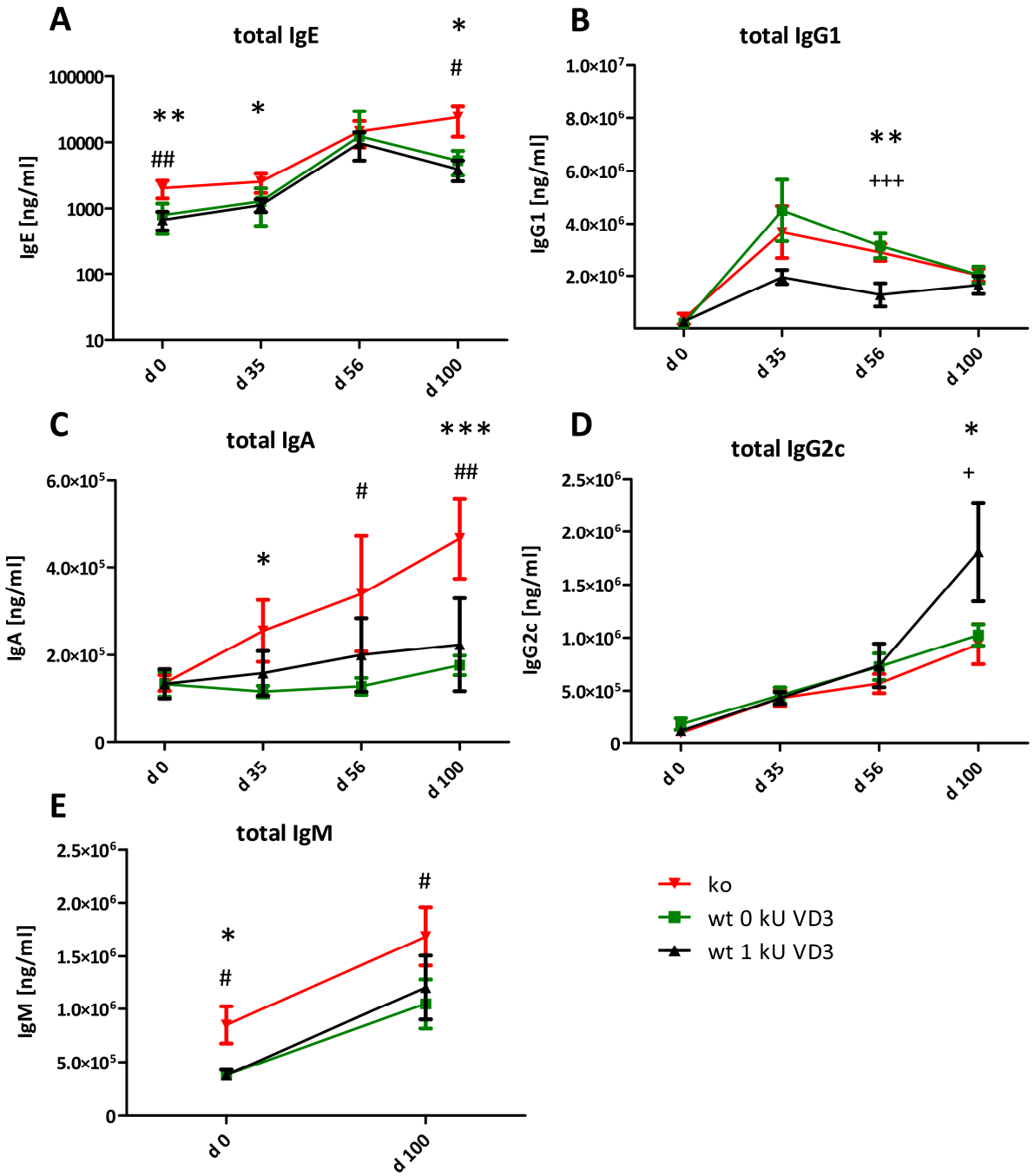

Figure 12. Serum immunoglobulin concentrations. IgE, IgG1, IgA, IgG2c and IgM were measured at days 0, 35, 56 and 100. IgM was only assessed at days 0 and 100. Data are shown as mean ± SEM (n≥8). * significant between the groups ko and wt 1 kU, # significant between the groups ko and wt 0 kU, + significant between the groups wt 0 kU and wt 1 kU.

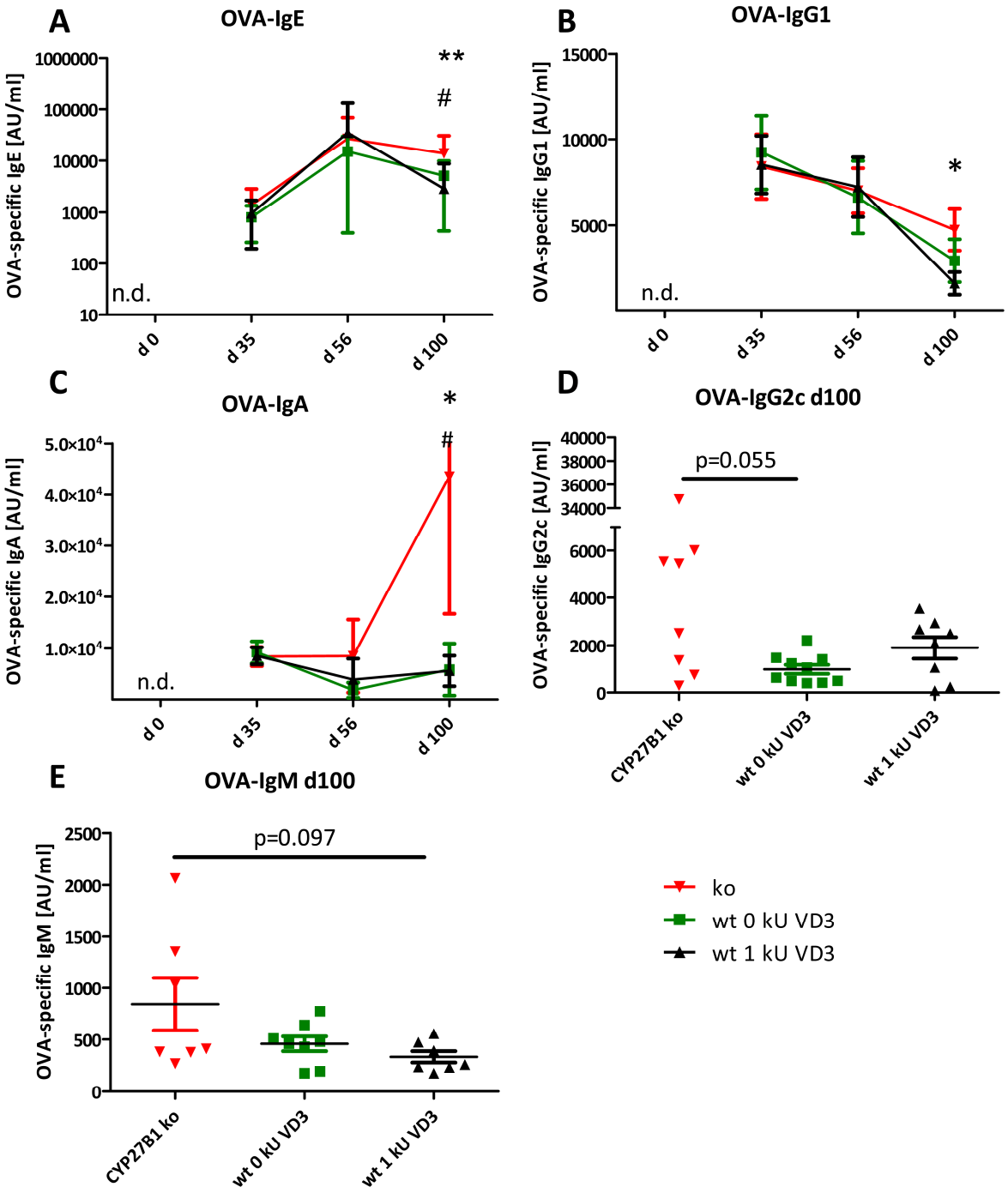

Figure 13. OVA-specific immunoglobulin serum concentration. OVA-specific IgE, IgG1, IgA, IgG2c and IgM were measured by ELISA. OVA-IgG2c was only detectable at day 100. OVA-IgM was only measured at day 100. Data are shown as mean ± SEM (n≥8). * significant between the groups ko and wt 1 kU, # significant between the groups ko and wt 0 kU. n.d. not detectable. AU: arbitrary units measured with a serum standard of pooled sera from sensitized mice.

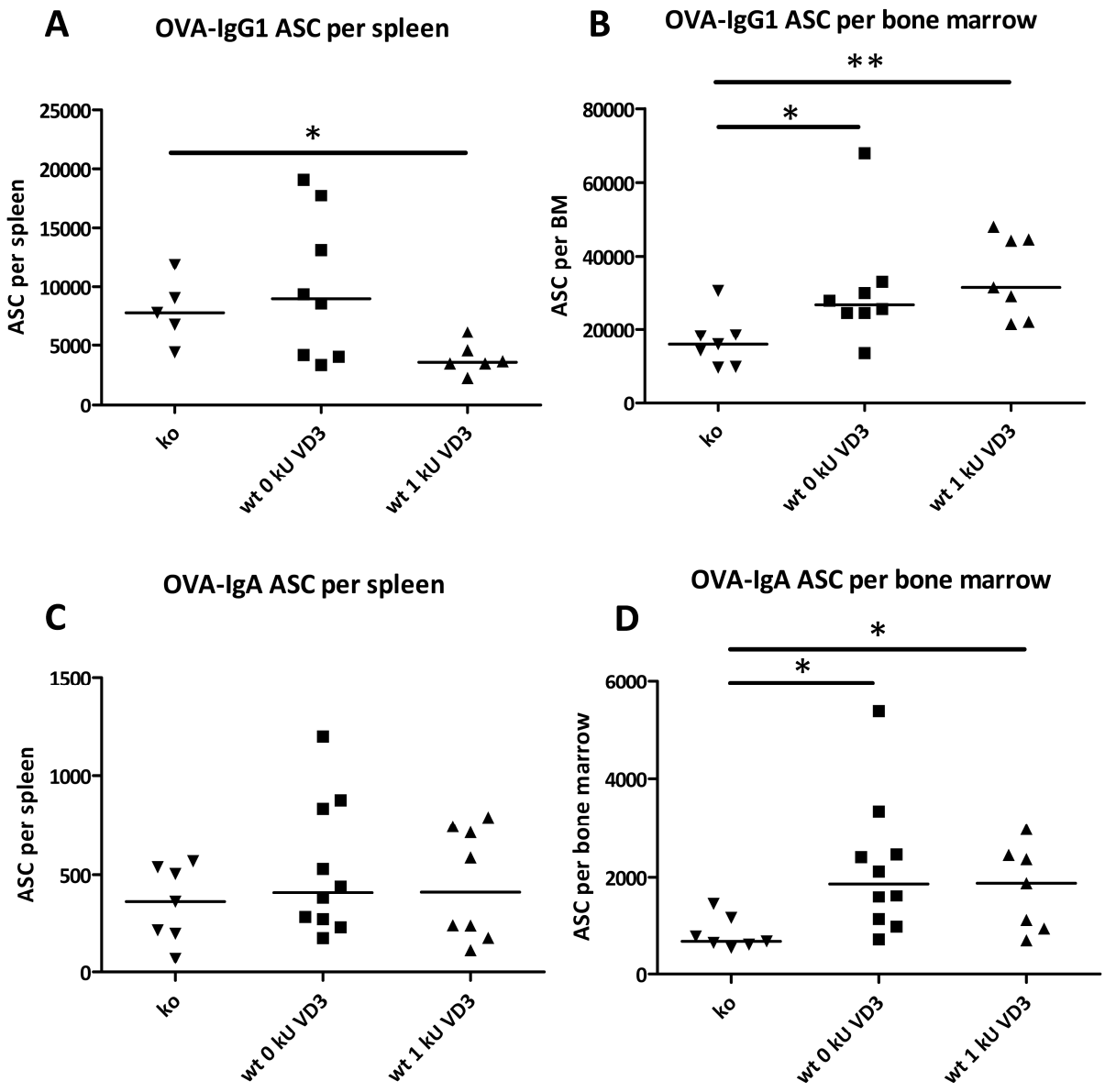

Figure 14. Lack of endogenous calcitriol production influences the number and location of antibody secreting cells. OVA-specific IgG1 and IgA ASC were measured by ELISPOT in spleen and bone marrow at day 100 and are shown as the median for each group (n≥7). Serial dilutions of single cell suspensions were incubated on OVA-coated filter plates. ASC can be detected as spots.

The numbers of OVA-IgA ACS were unchanged in the spleens of all groups. In contrast, CYP27B1$^{-/-}$ mice had significantly less OVA-IgA ACS in the bone marrow than wt mice (Figure 14C, D), as assessed by ELISPOT analysis. Total numbers of OVA-IgA ASC summed up from spleen and bone marrow were lower in CYP27B1$^{-/-}$ mice (1189 [625 – 3299] cells) than in wt mice (2303 [1121 – 3877] cells) like already seen for OVA-IgG1 ASC. OVA-IgE ASC were not measured due to limitations in terms of cell numbers.

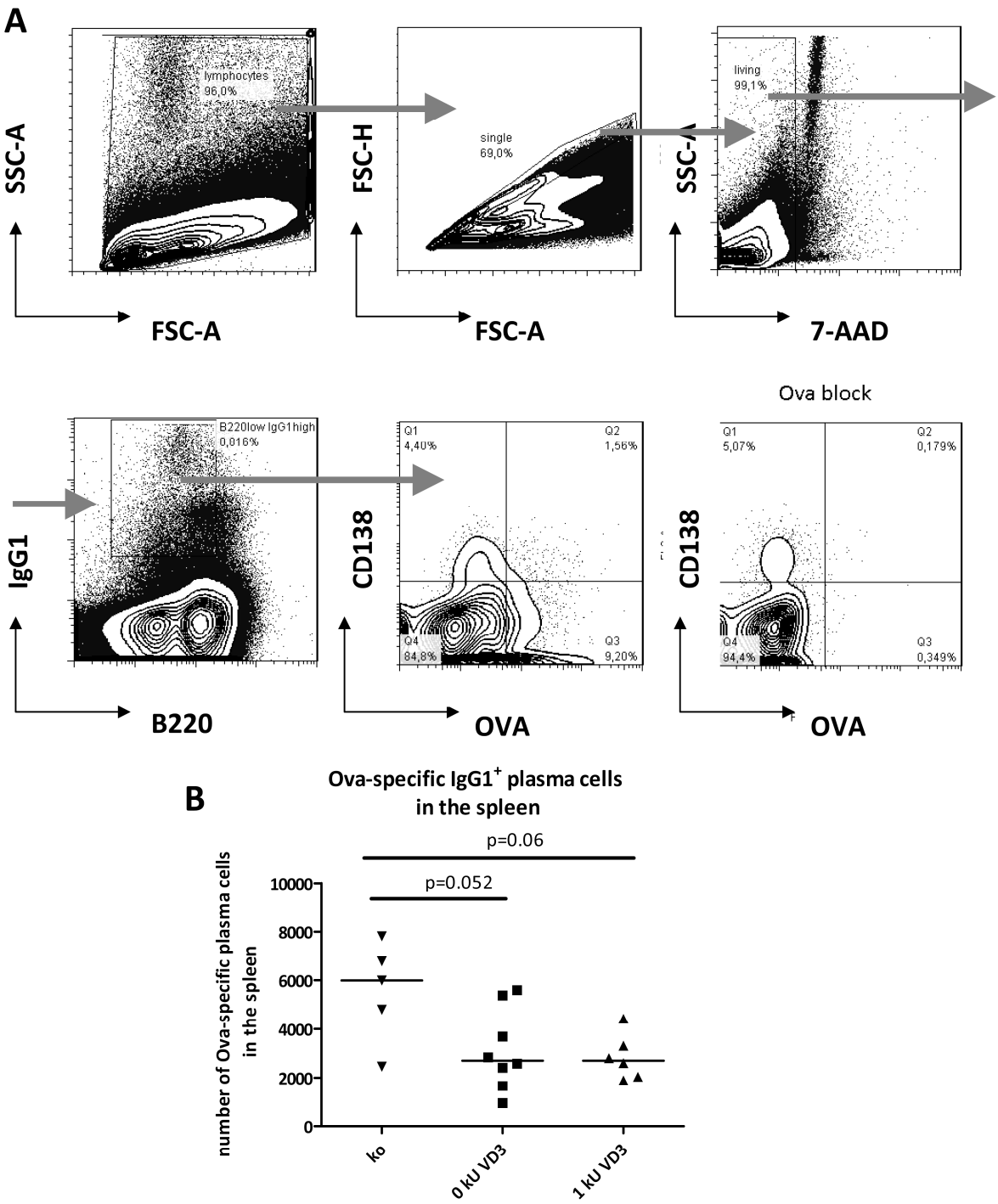

Figure 15. Numbers of OVA-specific IgG1^{+} plasma cells are increased in spleens of CYP27B1$^{-/-}$ mice. 2x10^{7} splenocytes were collected on a MACSQuant analyzer. **A.** Single cells were selected in a FSC-A/FSC-H dot plot. Dead cells were excluded as 7-AAD^{high}. Plasma blasts and plasma cells were defined as B220^{low}, IgG1^{+}, CD138^{+} and OVA^{+}. As a specificity control for the OVA-staining, staining was blocked with 1000-fold excess of unlabeled OVA. **B.** Cell numbers are shown as single values and the median for each group (n≥5).

7.2.4. Intact splenic architecture in CYP27B1$^{-/-}$ mice

To investigate whether the spleen structure and in particular the follicles are dependent on endogenous calcitriol production, CYP27B1$^{-/-}$ and wt mice were compared. Frozen spleen sections were stained with anti-B220 for the detection of B cells and anti-MOMA for marginal metallophillic macrophages residing in the marginal zone at the border of the follicles. Splenic architecture was normal in CYP27B1$^{-/-}$ mice (a representative picture is shown in Figure 16). The number and size of B cell follicles (red) were comparable, as well as B cell zones and unstained T cell zones. Marginal metallophillic macrophages (blue) were normally distributed.

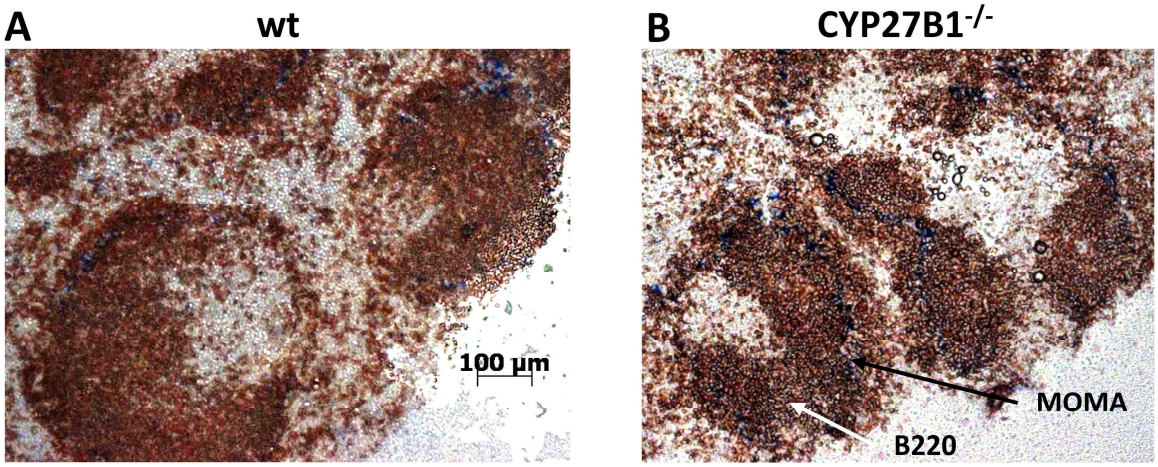

Figure 16. Normal follicular structure in CYP27B1$^{-/-}$ mice. Representative histological image of anti-B220 (red, indicated by white arrow) and anti-MOMA (blue, indicated by black arrow) stained 7 µm frozen spleen sections of CYP27B1$^{-/-}$ and wt mice. Images are shown at 100-fold magnification.

7.2.5. Lack of CYP27B1 expression alters the splenic B cell compartment

Although the overall splenic architecture remained unchanged in CYP27B1$^{-/-}$ mice, the B cell compartment was examined in more detail by flow cytometric analysis of splenic follicular (FO) and marginal zone (MZ) B cells. The gating strategy is shown in Figure 17A. B cells were gated as 7-AAD^{-} CD19^{+} lymphocytes. FO B cells are CD21^{+}, CD23^{+}, whereas MZ B cells are CD21^{high}, CD23^{-}. CYP27B1$^{-/-}$ mice had significantly lower numbers of CD19 B cells in the spleen (median: 3.8x10^{6} cells, range 1.97x10^{6} – 1.29x10^{6}) than VD deficient wt mice (median: 1.1x10^{7} cells, range: 5.7x10^{6} – 1.8x10^{7}, Figure 17B). By tendency, normal wt mice had more CD19 B cells than CYP27B1$^{-/-}$ mice, although the variation was too high to reach statistical significance (median: 8.7x10^{6} cells, range: 3x10^{6} – 3.6x10^{7}). Accordingly, numbers of FO and MZ B cells were also reduced in CYP27B1$^{-/-}$ mice (Figure 17C, D).

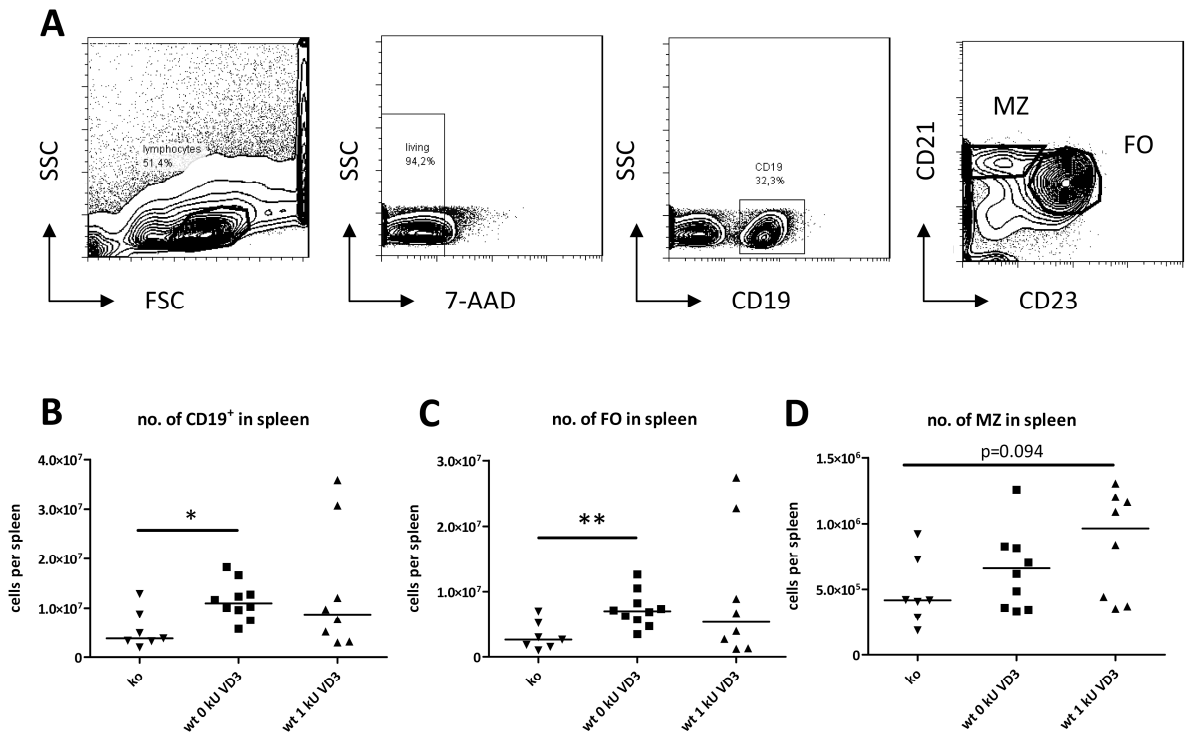

Figure 17. B cell numbers are reduced in spleens of CYP27$^{-/-}$ mice. A. Lymphocytes were selected in the forward and side scatter and dead cells were excluded by 7-AAD. B cells were gated as CD19^{+}. MZ and FO B cells are distinguished by their differential expression of CD21 and CD23. Numbers of **B.** CD19^{+}, **C.** FO and **D.** MZ B cells per spleen were analyzed. Data are shown as the median for each group (n≥8). * p≤0.05, ** p≤0.005.

7.2.6. Intact splenic T cell compartment in CYP27B$^{-/-}$ mice

The splenic T cell compartment was analyzed by flow cytometry at day 100 of the experiment as shown in Figure 18A. Lymphocytes were selected in the forward and side scatter and dead cells were excluded with 7-AAD. $CD3^+$ T cells were separately analyzed for $CD4^+$ and $CD8^+$ T cells. Naïve T cells expressing CD44 and high levels of CD62L, central memory (CM) T cells expressing CD62L and CD44 and effector memory (EM) T cells expressing CD44 but no CD62L were inverstigated.

The data show that numbers of $CD4^+$ and $CD8^+$ T cells were unchanged (Figure 18B, F). The $CD4^+$ T cell compartment was not significantly altered (Figure 18B-E). By tendency, naïve $CD4^+$ T cells were slightly increased (ko median: $5.8x10^6$, wt deficient wt: $3.9x10^6$, wt: $4.7x10^6$). Regarding $CD8^+$ T cells the memory compartment was slightly reduced in CYP27B1$^{-/-}$ mice (Figure 18H, I), this difference was most pronounced for EM T cells (ko median: $1.97x10^5$ cells, wt VD deficient: $3.47x10^5$ cells, wt: $3.19x10^5$ cells).

Since calcitriol is known to be an inducer of regulatory T cells (T_{reg}) in mice[36], this cell population was analyzed in CYP27B1$^{-/-}$ mice (Figure 19). Single lymphocytes were gated on $CD4^+$, $CD25^+$, $FoxP3^+$ T_{reg}. The specificity of the staining was controlled by a CD25 unstained sample and a FoxP3 isotype control. However, the numbers of $CD4^+$ T cells and T_{reg} were comparable in all groups (Figure 19B, C).

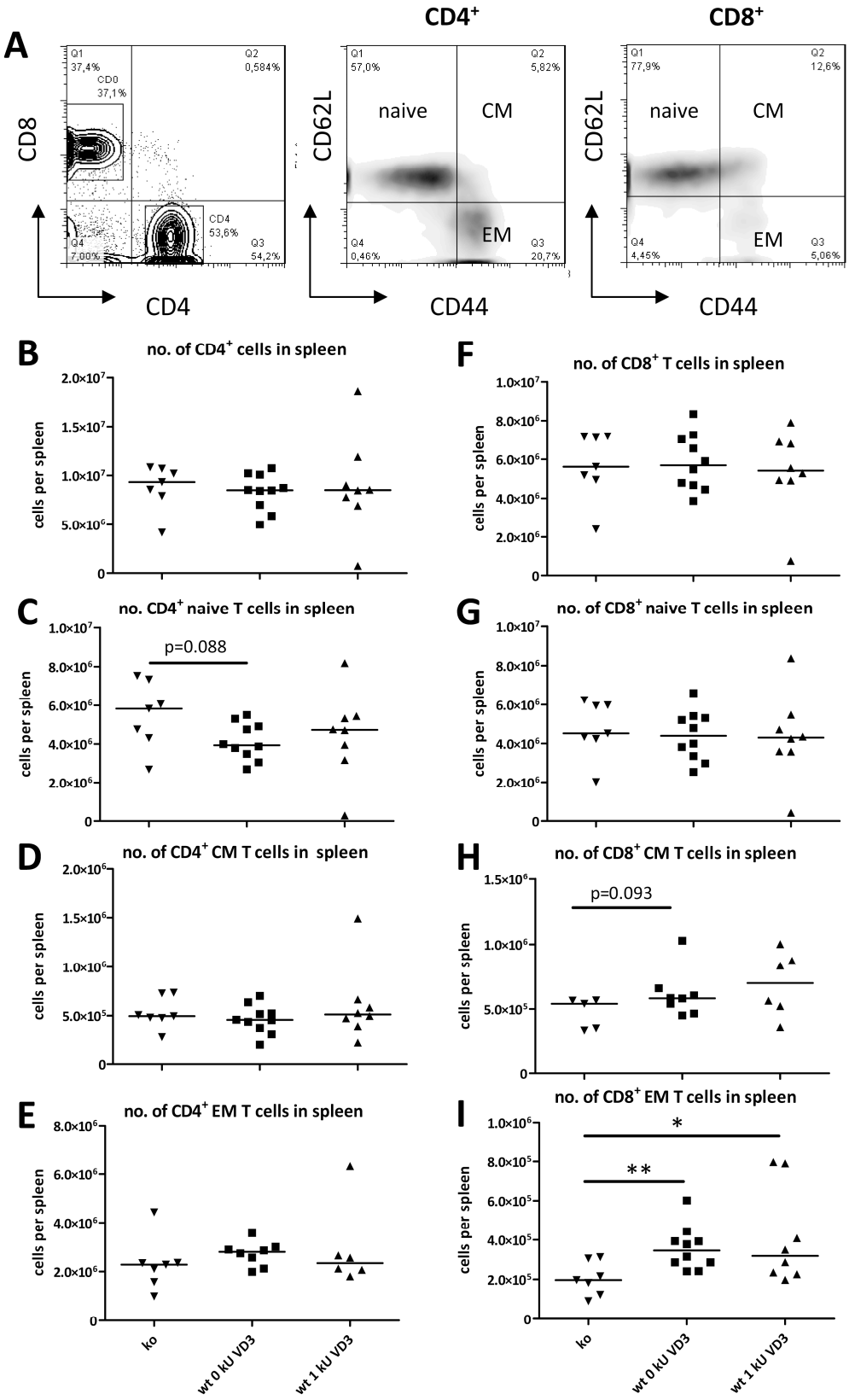

Figure 18. T cell numbers are not significantly affected in CYP27B1$^{-/-}$ mice. A. Lymphocytes were selected in the forward and side scatter and dead cells were excluded by 7-AAD. CD3$^+$ T cells were further gated for CD4$^+$ and CD8$^+$ T cells. CD44 and CD62L were used to differentiate between naïve (CD62L$^+$, CD44^{low}), central memory (CM, CD62L$^+$, CD44$^+$) and effector memory (EM, CD62$^-$, CD44$^+$) T cells. **B-E**. CD4$^+$ T cells. **F-I.** CD8$^+$ T cells. Data are shown as single values and the median for each group (n≥8). * p≤0.05, ** p≤0.005.

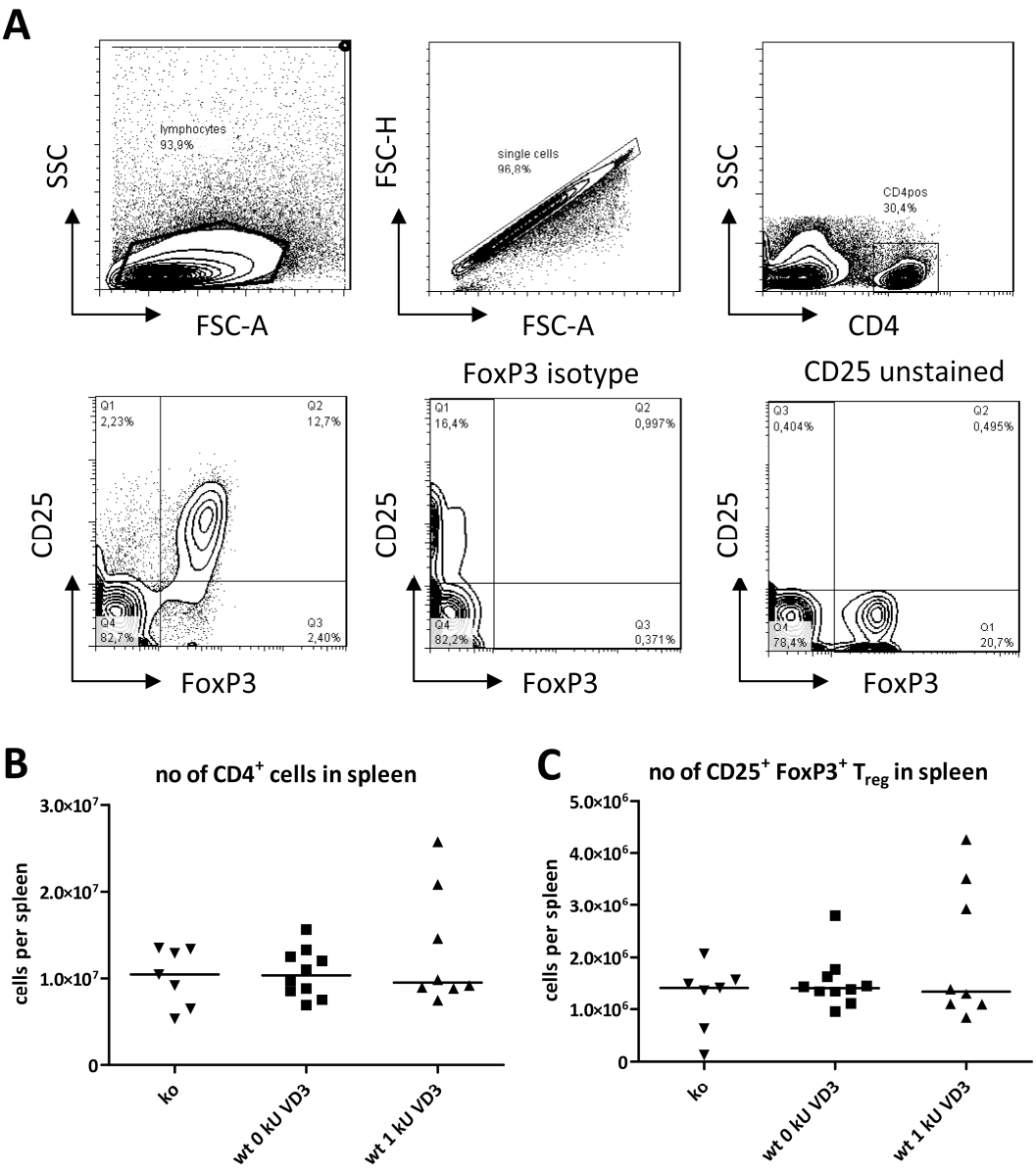

Figure 19. T_{reg} are not altered in CYP27$^{-/-}$ mice. A. Lymphocytes were selected in the forward and side scatter and dead cells were excluded with 7-AAD. $CD4^+$ T cells were gated on $CD25^+$, $FoxP3^+$ T_{reg}. The specificity of the staining was controlled with a CD25 unstained sample and a FoxP3 isotype control. The number of **B.** $CD4^+$ T cells and **C.** $CD4^+$, $CD25^+$, $FoxP3^+$ T_{reg} per spleen was analyzed and shown as single values and the median for each group (n≥8).

7.2.7. CYP27B1$^{-/-}$ mice display an increased cutaneous hypersensitivity reaction compared to wt mice

Symptoms of an allergic reaction are triggered by mast cells which bind IgE via FcεRI, but also IgG via FcγRII and FcγRIII. Upon cross linking of IgE and IgG, respectively, mast cells release mediators like histamine, prostaglandins and

leukotrienes resulting in increased vasopermeability and edema formation[77]. To study the biological relevance of the humoral immune response with respect to allergen-specific IgE and IgG1, a cutaneous hypersensitivity reaction (HSR) was measured after intradermal OVA challenge. Ear swelling was measured 2 h after OVA and NaCl injection and thereby reflects the early phase mast cell reaction. The cutaneous HSR was significantly higher in CYP27B1$^{-/-}$ than in VD-deficient wt mice (100.4 ± 27 µm versus 23.7 ± 13.9 µm) and also clearly more pronounced than in wt mice receiving a normal diet (100.4 ± 27 µm versus 46.6 ± 8.1 µm, Figure 20A). The cutaneous HSR correlated with allergen-specific IgE serum concentrations (r=0.5, p=0.006, Figure 20B) and with allergen-specific IgG1 serum concentrations (r=0.47, p=0.02, Figure 20C), indicating that both immunoglobulins are associated with the manifestation of an allergic response.

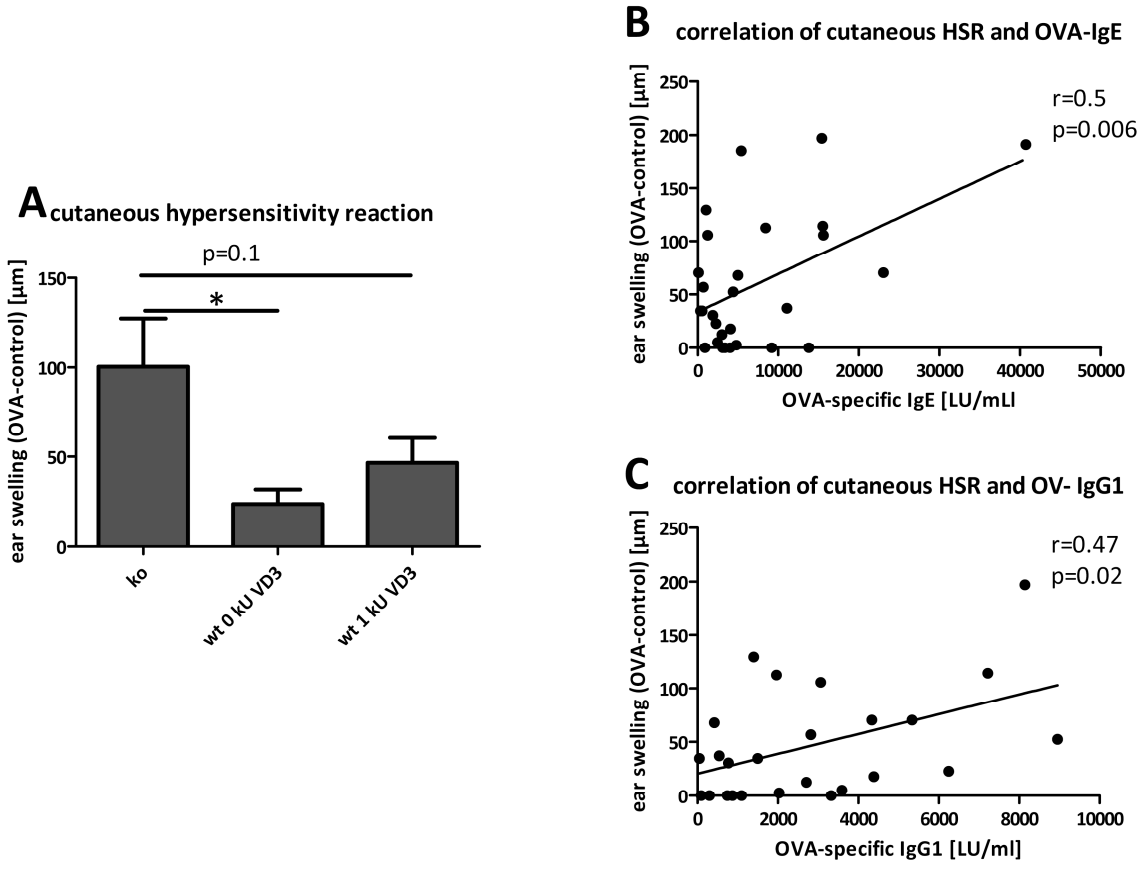

Figure 20. CYP27B1$^{-/-}$ mice have a more pronounced cutaneous hypersensitivity reaction than wt mice . A. 100 µg OVA dissolved in 20 µl PBS or vehicle were injected into the ear lobe. Ear thickness was measured before and 2 h after injection with a micrometer and swelling was determined as OVA(2 h – 0 h) - PBS(2 h – 0 h). Data are shown as mean + SEM. Correlation between ear swelling and **B.** OVA IgE serum concentrations or **C.** OVA IgG1 serum concentrations were analyzed by determining the Pearson coefficient r. * p≤0.05

8. DISCUSSION

8.1. Calcitriol impairs NF-κB activation in human naïve B cells

Calcitriol is known as an immunomodulator targeting various immune cells, including monocytes, macrophages, dendritic cells but also T- and B-lymphocytes, hence modulating both innate and adaptive immune responses[78]. Since vitamin D (VD) deficiency and asthma have common risk factors, such as westernized life style[79] and increased skin pigmentation[80, 81], a link between the rising asthma prevalence and low vitamin D has been hypothesized[78]. In a mouse model of allergic asthma calcitriol has been shown to enhance the beneficial effect of allergen immunotherapy[82]. One of the hallmarks of type-I allergic reactions is the increased class switch towards IgE[83], which is usually found only at low concentrations in the plasma but is enhanced in atopic persons. The differentiation of a B cell to an IgE producing cell is tightly regulated, one of the most important transcription factors being NF-κB p50[84]. This is supported by the fact that $p50^{-/-}$ mice show a clear reduction of IgE[85, 86], highlighting the central role of p50 in IgE production.

Previous data show that calcitriol reduces ε-germline transcript expression, IgE production and nuclear amount of NF-κB p50 after anti-CD40 and IL-4 stimulation in human B cells[46]. Hence we hypothesized that VDR activation impairs IgE class switch recombination via interference with the NF-κB pathway. The aim of this study was to elucidate the underlying mechanism of calcitriol mediated modulation of NF-κB activation.

Up to now, calcitriol is known to interfere with different NF-κB family members, but so far nothing is known about its impact on p50, one of the key molecules for IgE class switch recombination in B cells. In DCs the expression of RelB is transcriptionally downregulated by calcitriol[87, 88]. This involves binding of VDR/RXRα to a defined region in the RelB promoter and a calcitriol-dependent recruitment of HDAC3. It has been suggested that this occurs selectively in APCs[84]. A VDR-mediated inhibition of p65 activation has been shown in different cell types. In monocytes, calcitriol inhibits nuclear activity of p65[89]. Furthermore, fibroblasts lacking the VDR show increased p65 activity[90].

Herein, it is shown for the first time that NF-κB p105 and p50 protein expression is reduced by calcitriol in human naïve B cells and that this inhibition is regulated at the transcriptional level by the liganded VDR. p105 transcription is mainly regulated by members of the NF-κB family themselves, namely p65, p50 and c-Rel[74]. Although other transcription factors are probably involved as well, the importance of NF-κB is supported by the inhibition of PMA activation of the promoter by an NF-κB transdominant negative mutant[91]. Thus, reduced p65 translocation mediated by calcitriol as seen in this work may result in transcriptional downregulation of p105 after 24 h. A direct transcriptional regulation of p105 by the VDR is unlikely, since no VDRE in the p105 promoter has been identified so far. In silico promoter analyses using the program “MatInspector” did not reveal putative binding sites for the VDR.

As p65 is retained in the cytosol of cells by IκBα and IκBα degradation precedes p65 nuclear translocation, this important protein was analyzed thoroughly. The data show that in naive B cells IκBα protein expression and degradation are stable upon calcitriol stimulation and thus, p65 translocation is reduced by an IκBα independent mechanism. However, the VDR impact on IκBα in different cell types has been described heterogeneously, most likely due to cell specificity. VDR mediates increased IκBα expression in colon cancer cells[92], HL-60 leukemia cells[93], keratinocytes[94] and macrophages[94], whereas IκBα expression is stable in human proximal tubular epithelial cells[95]. In fibroblast, calcitriol is reported to activate NF-κB by inducing IκBα phosphorylation[96].

Alternatively, IκBα-independent retention of p65 in the cytosol was described by direct complex formation with VDR in mouse embryonic fibroblasts[97] and proximal tubular epithelial cells[95]. Thus, protein-protein-interactions between VDR and p65 may prevent p65 from translocating to the nucleus even after IκBα-degradation. Whether this mechanism might underly the inhibition of p65 nuclear translocation was analyzed by Co-IP. Following precipitation of the VDR, complex formation with p65 could not be verified here. Since such protein complexes have been shown in other cell types it cannot be excluded, that p65 has been precipitated along with the VDR but was under the detection limit of the western blot. Furthermore, most of the VDR is located in the nucleus of cells even in an unliganded state. Co-IP was performed with whole cell lysates, but only the cytosolic amount of VDR would be able to retain p65 in the cytosol. Co-IP was also performed in purified cytosolic extracts, but the VDR could not be precipitated. Since the protein amount of VDR in the cytosol is rather

low, the weak signal cannot be differentiated from the precipitating antibody heavy chain that is in the sample and runs at the same height of 50 kD. This problem was tried to be solved by crosslinking anti-VDR to a matrix, so that the antibody heavy chain does not elute together with the sample. Crosslinking led to inactivation of the antibody so that no protein was precipitated. Despite of the discussed potential technical limitations, it is also possible that VDR p65 interactions are cell specific. It can also be hypothesized, that the VDR interacts with molecules like importin α, which transport NF-κB into the nucleus[98, 99] and thereby interferes with p65 nuclear translocation indirectly. Indeed, the expression of several importins is downregulated in calcitriol treated human leukemia HL-60 cells[100].
ChIP analysis confirmed that the reduced amount of p65 mediated by calcitriol leads to a decreased p65 binding to the p105 promoter. At the p105 promoter as well as at the IκBα promoter that was used as a positive control, anti-CD40 stimulation, which induces p65 nuclear translocation, induced p65 binding. In both cases calcitriol treatment reduced p65 binding drastically. Therefore, p105 transcription that depends to a great extent on p65 activation is reduced. Impairment of p65 binding to the IκBα promoter did not result in reduced IκBα expression, but regulation of the IκBα promoter is certainly different from that of the p105 promoter, including the relevance of a different set of transcription factors.

In naïve B cells, VDR activation with calcitriol inhibited nuclear translocation of p65 by an IκBα independent mechanism. This resulted in reduced binding of p65 to the p105 promoter and subsequently to diminished expression of p105, thereby causing reduced protein levels of p105 as well as p50.

Costimulation via CD40 is an important signal for B cell survival, proliferation and isotype switching[101]. CD40 signaling results in NF-κB activation, including NF-κB p50, which is crucial for IgE class switch recombination. Calcitriol treatment of B cells results in profoundly reduced IgE production. Herein it is shown that calcitriol reduces NF-κB p65 signaling and consequently p105 transcription in human naïve B cells. Thus, vitamin D receptor signaling may reduce or prevent exaggerated activation of B cells and unwanted immune responses, e.g. in IgE dependent diseases such as allergic asthma.

8.2. Targeted inactivation of CYP27B1 influences the humoral immune response

CYP27B1$^{-/-}$ mice have originally been generated to create a model of pseudovitamin D-deficiency rickets (PDDR)[69]. In these mice the gene encoding CYP27B1, the enzyme that catalyzes the formation of bioactive calcitriol from its precursor 25(OH)VD_3, is inactivated. When fed with a standard diet, homozygous mutant mice are hypocalcemic, hypophosphatemic, hyperparathyroidic and have undetectable calcitriol levels in the serum[69]. Feeding mice with a rescue diet containing 2% calcium, 1.25% phosphorus and 20% lactose rescues the phenotype[70]. Normocalcemia is reestablished, but the femur size remains significantly smaller[70]. In accordance with the literature, lower size and body weight were also observed in this study. 25(OH)VD_3 serum concentration was enhanced in CYP27B1$^{-/-}$ mice receiving a diet with the normal amount of 1 kU/kg VD_3 since it cannot be metabolized to produce calcitriol[69]. In this study, mice were given a VD_3 free rescue diet to prevent signaling of 25(OH)VD_3 via the VDR[102]. CYP27B1$^{-/-}$ and wt mice receiving this rescue diet without VD_3 had significantly lower 25(OH)VD_3 serum concentrations than wt mice receiving a standard diet (60 ± 1.8 versus 67 ± 7 versus 102 ± 10 nM). However, the rescue diet did not result in undetectable serum concentrations of 25(OH)VD_3, probably due to residual VD_3 in the chow. The manufacturer guarantees a VD_3 amount below 0.2 kU/kg, which may still be enough to obtain the observed serum levels. Therefore, it cannot be excluded that formation of calcitriol and signaling via the VDR takes place in VD-deficient wt mice. 25(OH)VD_3 is a known VDR ligand with direct gene regulatory properties[102], even if it binds to the VDR approximately 50 times less effectively than calcitriol. In CYP27B1$^{-/-}$ mice signaling via the VDR may even be stronger in the absence of calcitriol as a competitor.

The influence of the inactivation of CYP27B1 on the immune system has not been analyzed in detail yet. The numbers of $CD3^+$ $CD4^+$ and $CD3^+$ $CD8^+$ T cells did not differ in the spleens of the analyzed mice. The data shown here are not in line with the data from Panda et al[50]. These authors described reduced numbers of both T cell subsets in the periphery of non- sensitized CYP27B1$^{-/-}$ mice[50]. However, peripheral T cell numbers were not analyzed herein. Considering both observations, a homing defect can be suspected, as the gut-homing receptors α4β7 and CCR9 are suppressed by calcitriol, while the skin homing receptor CCR10 is upregulated[23, 103].

Interestingly, VDR ko mice exhibit a defect in T cell homing to the small intestine caused by reduced expression of CCR9[104]. Consequently, IL10/VDR double-ko mice develop fulminating inflammatory bowel disease, which cannot be cured by adoptive transfer of VDR ko $CD4^+$ T cells, but only with wt cells. Thus, homing may be completely differently regulated in CYP27B1$^{-/-}$ mice compared to wt mice. CCR7 is important for T cells to leave the spleen and recirculate through the lymphatic system[105]. The influence of calcitriol on CCR7 expression on T cells is not known yet, but in future experiments it would be interesting to analyze whether homing receptors are responsible for the modified T cell distribution in CYP27B1$^{-/-}$ mice.

The composition of the T cell compartment regarding naïve and memory T cells was not much altered. Among $CD8^+$ T cells, CYP27B1$^{-/-}$ mice had less effector and central memory T cells then wt mice. When compared with T_{CM}, T_{EM} are characterized by rapid effector functions. $CD8^+$ T_{EM}, which were significantly reduced in CYP27B1$^{-/-}$ mice, produce IFNγ, IL-4, and IL-5 within hours following antigenic stimulation[106]. Thereby it would be interesting to analyze CYP27B1$^{-/-}$ mice in a virus infection model to explore whether an infection would be more persistent in mice lacking endogenous calcitriol production.
Also T_{reg} numbers remained unchanged. This is surprising, since calcitriol is a known inducer of T_{reg}[107-109] and IL-10 production of T_{reg} in humans. In NOD mice, treatment with a calcitriol analog blocked pancreatic infiltration of T_H1 cells, enhanced $CD4^+CD25^+$ T_{reg} cells, and arrested the progression of type-I diabetes[110]. On the other hand, whether VD deficiency is related to an unusually low T_{reg} number is unknown, however, the results of this work do not point towards such an effect.
T cells were only analyzed at day 100 of the experiment In a next step it will be interesting to analyze these T cell populations in non-sensitized mice, but also during the course of the immune response, as time-dependent influences may be revealed.

Immunohistochemical staining of B220 and MOMA in spleen sections showed that the overall splenic architecture of CYP27B1$^{-/-}$ mice is not altered in comparison to wt mice. This is supported by the intact splenic T cell compartment as assessed by flow cytometry. Additionally, a more detailed analysis of the splenic B cell compartment was performed. The number of $CD19^+$ B cells was reduced in CYP27B1$^{-/-}$ mice. Although these mice also had slightly reduced overall splenic cell numbers, this

cannot be the explanation for the reduction of B cells. As a consequence of reduced $CD19^+$ B cells, numbers of follicular and marginal zone B cells were also decreased although the ratio of these two cell types did not change, supporting the observation of regular splenic architecture as seen in histochemistry. To reveal the reason for the diminished B cell number, B cell development will have to be analyzed by examining bone marrow and spleen of non-sensitized mice and sensitized mice in the course of an immune response. This will also shed light on the reasons for the increased amounts of antibodies that were observed in this experiment even before sensitization. Regarding reduced B cell numbers in the spleens of $CYP27B1^{-/-}$ mice it will also be important to examine the homing behaviour of these cells by analysis of chemokine receptor expression.

The humoral immune response has been analyzed in $CYP27B1^{-/-}$ mice with C57BL/6 background. In some disease models, differences between mouse strains have been observed. Regarding their response in an OVA induced type-I immune reaction, which is characterized by the T_H2 associated immunoglobulins IgE and IgG1, BALB/c mice have been identified as high responders, while C57BL/6 mice are low responders[111]. Therefore, BALB/c mice are usually preferred to analyze type-I immune responses. Strikingly, non-sensitized $CYP27B1^{-/-}$ mice had enhanced IgE and IgM serum concentrations, while IgG1, IgG2c and IgA concentrations were comparable to wt mice. IgE concentrations were measurable in ko and wt mice, showing that type-I immune responses can be well assessed in this mouse model.
During the course of a type-I immune response elicited by OVA sensitization both, IgE and IgM, were continuously enhanced in $CYP27B1^{-/-}$ mice. In line with the data presented here, Wittke et al showed that total and OVA-specific IgE are enhanced in VDR ko mice before and after OVA sensitization[112]. Other immunoglobulins were not analyzed in their work. However, a general enhancement of all immunoglobulin concentrations or a T_H1 or T_H2 related pattern was not observed. All OVA-specific isotypes were only significantly upregulated in $CYP27B1^{-/-}$ mice at day 100 of the experiment, when no acute immune response is ongoing. This suggests that the regulation of the immune response is disturbed in a way that the decline of immunoglobulin production after antigen exposure is delayed, or maybe exaggerated Immunoglobulin production as seen in autoimmunity. Notably, a defect in CYP27B1 upregulation in macrophages by immune stimuli like IFNγ was found in autoimmune

non-obese diabetic mice. Therefore, the upregulation of CYP27B1 in activated macrophages or other immune cells, resulting in the synthesis of calcitriol, might be a negative feedback loop in inflammation. A defect in this system might be an additional element in tipping the balance towards autoimmunity[113]. Therefore, the analysis of autoantibodies, e.g. anti-nuclear antibodies will shed light on self-pathogenic processes.

Interestingly, decreased calcitriol serum concentrations have been reported in many autoimmune diseases, including SLE[22]. Since SLE is characterized by an immune dysregulation resulting in an overproduction of autoantibodies, Chen et al hypothesized that calcitriol deficiency may contribute to B cell hyperreactivity[21]. Vitamin D deficiency may promote autoimmunity by favoring the inordinate production of T_H17 and T_H9 cells[114]. The significantly altered humoral immune response observed in CYP27B1$^{-/-}$ supports this hypothesis. Strikingly, the immunoglobulin profile of VD-deficient wt mice is more similar to that of normal wt mice than to that of CYP27B1$^{-/-}$ mice. This may be due to the above mentioned serum concentrations of 25(OH)VD_3 and its conversion into calcitriol. It also has been reported that calcitriol and 25(OH)VD_3 can act synergistically to elicit stronger responses than one VDR agonist alone[102]. Although calcitriol concentrations were not measured it can be assumed, that calcitriol is produced as long as 25(OH)VD_3 is present in the serum. Therefore, the humoral immune response of VD deficient wt mice may not be as strongly affected as that of CYP27B1$^{-/-}$ mice.

It has been shown previously, that calcitriol promotes the T_H2 response, while suppressing the T_H1 response. Bone marrow macrophages from VDR ko mice produce less IL-18 and IL-12, while splenocytes from these mice produce less IFNγ and more IL-4[113, 114]. Generally, in the absence of vitamin D signaling, the T cell compartment is reported to have a potentially stronger T_H1 phenotype[115]. On the contrary, in allergic bronchopulmonary aspergillosis, which is caused by a dominant T_H2 immune response to antigens derived from the opportunistic mold *Aspergillus*, heightened T_H2 reactivity is correlated with lower mean serum vitamin D levels[116]. Calcitriol modulates the T_H1/T_H2 balance; in its absence, this balance is out of equilibrium, probably resulting in an unusual antibody pattern as observed herein. Although the antibody pattern did not reflect a typical T_H2 profile, elevated IgE levels of non-sensitized mice as well as during the course of the immune response

triggered by OVA suggests that CYP27B1$^{-/-}$ mice may be more T_H2 prone than their wt littermates. To analyze this hypothesis in more detail, it would be interesting to analyze T_H1 and T_H2 related cytokine production by T cells isolated from spleen and lymph nodes of sensitized and non-sensitized mice, either by FACS analysis or in cell culture supernatants after *in vitro* restimulation. It would also be of interest to perferm these experiments with T cells isolated earlier after sensitization that reflect the ongoing immune response.

CYP27B1$^{-/-}$ mice had more OVA-specific IgG1 and IgA at day 100, which was not reflected by the number of specific ASC in spleen and bone marrow, as determined by ELISPOT. Ko mice had more OVA-specific IgG1 ASC in the spleen and less in the bone marrow than wt mice. If cell numbers from spleen and bone marrow are summed up, ko mice have less OVA-specific IgG1 ASC in total. Numbers of OVA-specific IgA ASC in the spleen were comparable in all groups, whereas they are lower in the bone marrow of ko mice. Calcitriol has been reported to upregulate the chemokine receptor CXCR4[117]. In chimeric mice reconstituted with fetal liver cells from CXCR4$^{-/-}$ mice, plasma cells failed to normally populate the bone marrow whereas their numbers did not change in the spleen and accumulated in the blood, indicating that CXCR4 is important for regular homing to the bone marrow but not important to migrate from the spleen[118]. Thus, plasma cell homing to the bone marrow may be disturbed in CYP27B1$^{-/-}$ mice, accounting for reduced numbers of IgG1 and IgA ASC in the bone marrow of ko mice. However, spleen and bone marrow are not the only organs where plasma cells reside. As mentioned above, they can accumulate in the blood, but more importantly, they can also reside in secondary lymphoid organs like lymph nodes or the mucosa of the gastrointestinal tract. Both compartments have not been analyzed herein. Mice have been sensitized i.p., which triggers an immune response in the mesenteric lymph nodes. High levels of total and OVA-specific IgA may originate from ASC residing in the gut. Calcitriol suppresses the gut-homing receptors α4β7 and CCR9[22], so that gut homing may preferentially occur in CYP27B1$^{-/-}$ mice. It will thereby be interesting to analyze, whether IgA-secreting plasma cells reside in the gut or mesenteric lymph nodes of ko mice.

The cutaneous HSR following intradermal OVA challenge was much stronger in CYP27B1$^{-/-}$ mice than in their wt littermates. Ear swelling is evoked by degranulation

of mast cells. On their surfaces, IgE and IgG1 are cross linked by OVA following release of mast cell mediators like histamine and prostaglandins that lead to increased vasopermeability[77]. Besides IgE, IgG1 is a potent inducer of mast cell degranulation in mice[119]. The early phase reaction peaks after 20 min, but is detectable for a few hours. It was not possible to measure ear swelling earlier than 2 h after challenge due to the wheal caused by the injection of a relatively large volume of fluid. The increased cutaneous HSR in CYP27B1$^{-/-}$ mice is associated with OVA-specific IgE (r=0.5) and IgG1 (r=0.47) serum concentrations. Therefore, enhanced immunoglobulin production observed in CYP27B1$^{-/-}$ mice has functional consequences regarding the manifestation of a clinical parameter of the type-I immune response. This is in line with the finding that lower serum 25(OH)VD_3 correlates with increased severity of allergic asthma[45].

Taken together, CYP27B1$^{-/-}$ mice which are not capable to produce calcitriol endogenously, showed a significantly altered immunoglobulin profile in a non-sensitized state and after type-I sensitization with OVA/alum. The immunoglobulin pattern did neither reflect a distinct T_H1 nor a T_H2 shift; although enhanced IgE titers suggest that the T_H2 response is elevated. It rather implied a general failure in the regulation of the humoral immune response, as all OVA-specific immunoglobulins were enhanced at day 100 after the initial sensitization. OVA-specific plasma cell numbers in spleen and bone marrow were not increased, suggesting a modified homing of cells in CYP27B1$^{-/-}$ mice, as plasma cells can also reside in lymph nodes and mucosal sites. B cell numbers were reduced in CYP27B1$^{-/-}$ mice, while the T cell subsets were basically unchanged, except the reduced $CD8^+$ T_{EM} population. CYP27B1$^{-/-}$ mice reacted stronger in a functional OVA induced cutaneous HSR, correlating with enhanced OVA-specific IgE and IgG1 in the serum.

In their role APCs, DCs effectively activate antigen-presenting T cells in lymphoid tissues[120]. Upon calcitriol stimulation DCs express reduced levels of MHC class II and the costimulatory molecules CD80 and CD86[121]. Furthermore, the release of proinflammatory cytokines like IL-12 and TNFα is inhibited, while IL-10 production is increased by calcitriol[121]. Therefore calcitriol action on DCs induces a delicate immune balance[34, 122].

The results obtained in CYP27B1$^{-/-}$ mice support the hypothesis that calcitriol is an important immune modulator and that the VD status as assessed by serum 25(OH)VD_3 has an impact on B cell homeostasis.

9. LITERATURE

1. Holick, M.F. The Cutaneous Photosynthesis of Previtamin D3: A Unique Photoendocrine System. *J Investig Dermatol* **77**, 51-58 (1981).
2. MacLaughlin, J.A., Anderson, R.R. & Holick, M.F. Spectral character of sunlight modulates photosynthesis of previtamin D3 and its photoisomers in human skin. *Science* **216**, 1001-1003 (1982).
3. Searing, D.A. & Leung, D.Y. Vitamin D in atopic dermatitis, asthma and allergic diseases. *Immunol Allergy Clin North Am* **30**, 397-409.
4. Jones, G., Strugnell, S.A. & DeLuca, H.F. Current understanding of the molecular actions of vitamin D. *Physiol Rev* **78**, 1193-1231 (1998).
5. Holick, M.F. Resurrection of vitamin D deficiency and rickets. *J Clin Invest* **116**, 2062-2072 (2006).
6. Haussler, M.R. *et al.* Vitamin D receptor: molecular signaling and actions of nutritional ligands in disease prevention. *Nutrition Reviews* **66**, S98-S112 (2008).
7. Aranda, A. & Pascual, A. Nuclear Hormone Receptors and Gene Expression. *Physiol. Rev.* **81**, 1269-1304 (2001).
8. Issa, L.L., Leong, G.M. & Eisman, J.A. Molecular mechanism of vitamin D receptor action. *Inflamm Res* **47**, 451-475 (1998).
9. Mizwicki, M.T. & Norman, A.W. The vitamin D sterol-vitamin D receptor ensemble model offers unique insights into both genomic and rapid-response signaling. *Sci Signal* **2**, re4 (2009).
10. Wang, T.-T. *et al.* Large-Scale in Silico and Microarray-Based Identification of Direct 1,25-Dihydroxyvitamin D3 Target Genes. *Mol Endocrinol* **19**, 2685-2695 (2005).
11. Barsony, J. & Prufer, K. Vitamin D receptor and retinoid X receptor interactions in motion. *Vitam Horm* **65**, 345-376 (2002).
12. Polly, P. *et al.* VDR-Alien: a novel, DNA-selective vitamin D3 receptor-corepressor partnership. *The FASEB Journal* **14**, 1455-1463 (2000).
13. Tagami, T., Lutz, W.H., Kumar, R. & Jameson, J.L. The Interaction of the Vitamin D Receptor with Nuclear Receptor Corepressors and Coactivators. *Biochem Biophys Res Commun* **253**, 358-363 (1998).
14. Sanchez-Martinez, R., Zambrano, A., Castillo, A.I. & Aranda, A. Vitamin D-dependent recruitment of corepressors to vitamin D/retinoid X receptor heterodimers. *Mol Cell Biol* **28**, 3817-3829 (2008).
15. Carlberg, C. & Polly, P. Gene regulation by vitamin D3. *Crit Rev Eukaryot Gene Expr* **8**, 19-42 (1998).
16. Kremer, R. *et al.* Identification and Characterization of 1,25-Dihydroxyvitamin D3-responsive Repressor Sequences in the Rat Parathyroid Hormone-related Peptide Gene. *J Biol Chem* **271**, 16310-16316 (1996).
17. Murayama, A., Kim, M.S., Yanagisawa, J., Takeyama, K. & Kato, S. Transrepression by a liganded nuclear receptor via a bHLH activator through co-regulator switching. *EMBO J* **23**, 1598-1608 (2004).
18. Turunen, M.M., Dunlop, T.W., Carlberg, C. & Vaisanen, S. Selective use of multiple vitamin D response elements underlies the 1 alpha,25-dihydroxyvitamin D3-mediated negative regulation of the human CYP27B1 gene. *Nucleic Acids Res* **35**, 2734-2747 (2007).

19. Fleet, J.C. Rapid, Membrane-Initiated Actions of 1,25 Dihydroxyvitamin D: What Are They and What Do They Mean? *J Nutr* **134**, 3215-3218 (2004).
20. Mora, J.R., Iwata, M. & von Andrian, U.H. Vitamin effects on the immune system: vitamins A and D take centre stage. *Nat Rev Immunol* (2008).
21. Chen, S. *et al.* Modulatory effects of 1,25-dihydroxyvitamin D3 on human B cell differentiation. *J Immunol* **179**, 1634-1647 (2007).
22. Sigmundsdottir, H. *et al.* DCs metabolize sunlight-induced vitamin D3 to 'program' T cell attraction to the epidermal chemokine CCL27. *Nat Immunol* **8**, 285-293 (2007).
23. Fritsche, J., Mondal, K., Ehrnsperger, A., Andreesen, R. & Kreutz, M. Regulation of 25-hydroxyvitamin D3-1{alpha}-hydroxylase and production of 1{alpha},25-dihydroxyvitamin D3 by human dendritic cells. *Blood* **102**, 3314-3316 (2003).
24. Bouillon, R. *et al.* Vitamin D and human health: lessons from vitamin D receptor null mice. *Endocr Rev* **29**, 726-776 (2008).
25. Stoffels, K. *et al.* Immune Regulation of 25-Hydroxyvitamin-D3-1α-Hydroxylase in Human Monocytes. *J Bone Miner Res* **21**, 37-47 (2006).
26. Alroy, I., Towers, T.L. & Freedman, L.P. Transcriptional repression of the interleukin-2 gene by vitamin D3: direct inhibition of NFATp/AP-1 complex formation by a nuclear hormone receptor. *Mol. Cell. Biol.* **15**, 5789-5799 (1995).
27. Takeuchi, A. *et al.* Nuclear factor of activated T cells (NFAT) as a molecular target for 1alpha,25-dihydroxyvitamin D3-mediated effects. *J Immunol* **160**, 209-218 (1998).
28. Cippitelli, M. & Santoni, A. Vitamin D3: a transcriptional modulator of the interferon-γ gene. *Eur J Immunol* **28**, 3017-3030 (1998).
29. Boonstra, A. *et al.* 1Î±,25-Dihydroxyvitamin D3 Has a Direct Effect on Naive CD4+ T Cells to Enhance the Development of Th2 Cells. *The Journal of Immunology* **167**, 4974-4980 (2001).
30. Staeva-Vieira, T.P. & Freedman, L.P. 1,25-Dihydroxyvitamin D3 Inhibits IFN-gamma and IL-4 Levels During In Vitro Polarization of Primary Murine CD4+ T Cells. *J Immunol* **168**, 1181-1189 (2002).
31. D'Ambrosio, D. *et al.* Inhibition of IL-12 production by 1,25-dihydroxyvitamin D3. Involvement of NF-kappaB downregulation in transcriptional repression of the p40 gene. *J Clin Invest* **101**, 252-262 (1998).
32. Etten, E.v. & Mathieu, C. Immunoregulation by 1,25-dihydroxyvitamin D3: Basic concepts. *J Steroid Biochem Mol Biol* **97**, 93-101 (2005).
33. Griffin, M.D., Xing, N. & Kumar, R. Vitamin D and its analogs as regulators of immune activation and antigen presentation. *Annu Rev Nutr* **23**, 117-145 (2003).
34. Bartels, L.E., Hvas, C.L., Agnholt, J., Dahlerup, J.F. & Agger, R. Human dendritic cell antigen presentation and chemotaxis are inhibited by intrinsic 25-hydroxy vitamin D activation. *Int Immunopharmacol* **10**, 922-928 (2010).
35. Bikle, D. Nonclassic actions of vitamin D. *J Clin Endocrinol Metab* **94**, 26-34 (2009).
36. Daniel, C., Sartory, N.A., Zahn, N., Radeke, H.H. & Stein, J.M. Immune Modulatory Treatment of Trinitrobenzene Sulfonic Acid Colitis with Calcitriol Is Associated with a Change of a T Helper (Th) 1/Th17 to a Th2 and Regulatory T Cell Profile. *J Pharmacol Exp Ther* **324**, 23-33 (2008).
37. Hyppönen, E., Läärä, E., Reunanen, A., Järvelin, M.-R. & Virtanen, S.M. Intake of vitamin D and risk of type 1 diabetes: a birth-cohort study. *The Lancet* **358**, 1500-1503 (2001).
38. Munger, K.L., Levin, L.I., Hollis, B.W., Howard, N.S. & Ascherio, A. Serum 25-Hydroxyvitamin D Levels and Risk of Multiple Sclerosis. *JAMA* **296**, 2832-2838 (2006).

39. Merlino, L.A. *et al.* Vitamin D intake is inversely associated with rheumatoid arthritis: Results from the Iowa Women's Health Study. *Arthritis Rheum* **50**, 72-77 (2004).
40. Cantorna, M.T. Vitamin D and its role in immunology: Multiple sclerosis, and inflammatory bowel disease. *Prog Biophys Mol Biol* **92**, 60-64 (2006).
41. Lange, N.E., Litonjua, A., Hawrylowicz, C.M. & Weiss, S. Vitamin D, the immune system and asthma. *Expert Rev Clin Immunol* **5**, 693-702 (2009).
42. Topilski, I. *et al.* The anti-inflammatory effects of 1,25-dihydroxyvitamin D3 on Th2 cells in vivo are due in part to the control of integrin-mediated T lymphocyte homing. *Eur J Immunol* **34**, 1068-1076 (2004).
43. Matheu, V., Back, O., Mondoc, E. & Issazadeh-Navikas, S. Dual effects of vitamin D-induced alteration of TH1/TH2 cytokine expression: enhancing IgE production and decreasing airway eosinophilia in murine allergic airway disease. *J Allergy Clin Immunol* **112**, 585-592 (2003).
44. Hypponen, E., Berry, D.J., Wjst, M. & Power, C. Serum 25-hydroxyvitamin D and IgE - a significant but nonlinear relationship. *Allergy* (2009).
45. Brehm, J.M. *et al.* Serum Vitamin D Levels and Markers of Severity of Childhood Asthma in Costa Rica. *Am J Respir Crit Care Med* (2009).
46. Heine, G., Anton, K., Henz, B.M. & Worm, M. 1alpha,25-dihydroxyvitamin D3 inhibits anti-CD40 plus IL-4-mediated IgE production in vitro. *Eur J Immunol* **32**, 3395-3404 (2002).
47. Milovanovic, M. *et al.* Vitamin D receptor binds to the [epsilon] germline gene promoter and exhibits transrepressive activity. *J Allergy Clin Immunol* **Nov;126(5):1016-23** (2010).
48. Torkildsen, O., Knappskog, P.M., Nyland, H.I. & Myhr, K.-M. Vitamin D-Dependent Rickets as a Possible Risk Factor for Multiple Sclerosis. *Arch Neurol* **65**, 809-811 (2008).
49. Lopez, E.R. *et al.* A promoter polymorphism of the CYP27B1 gene is associated with Addison's disease, Hashimoto's thyroiditis, Graves' disease and type 1 diabetes mellitus in Germans. *Eur J Endocrinol* **151**, 193-197 (2004).
50. Panda, D.K. *et al.* Targeted ablation of the 25-hydroxyvitamin D 1alpha -hydroxylase enzyme: evidence for skeletal, reproductive, and immune dysfunction. *Proc Natl Acad Sci U S A* **98**, 7498-7503 (2001).
51. Bonizzi, G. & Karin, M. The two NF-kappaB activation pathways and their role in innate and adaptive immunity. *Trends Immunol* **25**, 280-288 (2004).
52. Oeckinghaus, A. & Ghosh, S. The NF-kappaB family of transcription factors and its regulation. *Cold Spring Harb Perspect Biol* **1**, a000034 (2009).
53. Beinke, S. & Ley, S.C. Functions of NF-kappaB1 and NF-kappaB2 in immune cell biology. *Biochem J* **382**, 393-409 (2004).
54. Perkins, N.D. Integrating cell-signalling pathways with NF-kappaB and IKK function. *Nat Rev Mol Cell Biol* **8**, 49-62 (2007).
55. Thompson, J.E., Phillips, R.J., Erdjument-Bromage, H., Tempst, P. & Ghosh, S. I[kappa]B-[beta] regulates the persistent response in a biphasic activation of NF-[kappa]B. *Cell* **80**, 573-582 (1995).
56. Weil, R., Laurent-Winter, C. & Israel, A. Regulation of IkappaBbeta Degradation. *J Biol Chem* **272**, 9942-9949 (1997).
57. Whiteside, S.T., Epinat, J.-C., Rice, N.R. & Israel, A. I kappa B epsilon, a novel member of the I[kappa]B family, controls RelA and cRel NF-[kappa]B activity. *Embo J* **16**, 1413-1426 (1997).

58. Grewal, I.S. & Flavell, R.A. CD40 and CD154 in cell-mediated immunity. *Annu Rev Immunol* **16**, 111-135 (1998).
59. Elgueta, R. *et al.* Molecular mechanism and function of CD40/CD40L engagement in the immune system. *Immunol Rev* **229**, 152-172 (2009).
60. Dejardin, E. The alternative NF-[kappa]B pathway from biochemistry to biology: Pitfalls and promises for future drug development. *Biochem Pharmacol* **72**, 1161-1179 (2006).
61. Bishop, G.A. The multifaceted roles of TRAFs in the regulation of B-cell function. *Nat Rev Immunol* **4**, 775-786 (2004).
62. Zarnegar, B. *et al.* Unique CD40-mediated biological program in B cell activation requires both type 1 and type 2 NF-kappaB activation pathways. *Proc Natl Acad Sci U S A* **101**, 8108-8113 (2004).
63. Sasaki, Y. *et al.* Canonical NF-kappaB Activity, Dispensable for B Cell Development, Replaces BAFF-Receptor Signals and Promotes B Cell Proliferation upon Activation. *Immunity* **24**, 729-739 (2006).
64. Sun, S.C. & Ley, S.C. New insights into NF-kappaB regulation and function. *Trends Immunol* **29**, 469-478 (2008).
65. Agematsu, K., Hokibara, S., Nagumo, H. & Komiyama, A. CD27: a memory B-cell marker. *Immunol Today* **21**, 204-206 (2000).
66. Orlando, V. Mapping chromosomal proteins in vivo by formaldehyde-crosslinked-chromatin immunoprecipitation. *Trends Biochem Sci* **25**, 99-104 (2000).
67. Hsueh, R.C., Tamara I. A. Roach, Keng-Mean Lin, Timothy D. O´Conell, Heping Han, Zhen Yan Purification and Characterization of Mouse Splenic B Lymphocytes. *AfCS Research Reports* **Vol 1, No 1 BC**, 1-11 (2002).
68. Czerkinsky, C.C., Nilsson, L.-Å., Nygren, H., Ouchterlony, Ö. & Tarkowski, A. A solid-phase enzyme-linked immunospot (ELISPOT) assay for enumeration of specific antibody-secreting cells. *J Immunol Methods* **65**, 109-121 (1983).
69. Dardenne, O., Prud'homme, J., Arabian, A., Glorieux, F.H. & St-Arnaud, R. Targeted inactivation of the 25-hydroxyvitamin D(3)-1(alpha)-hydroxylase gene (CYP27B1) creates an animal model of pseudovitamin D-deficiency rickets. *Endocrinology* **142**, 3135-3141 (2001).
70. Dardenne, O., Prud'homme, J., Glorieux, F.H. & St-Arnaud, R. Rescue of the phenotype of CYP27B1 (1alpha-hydroxylase)-deficient mice. *J Steroid Biochem Mol Biol* **89-90**, 327-330 (2004).
71. Chervenick, P.A., Boggs, D.R., Marsh, J.C., Cartwright, G.E. & Wintrobe, M.M. Quantitative studies of blood and bone marrow neutrophils in normal mice. *Am J Physiol* **215**, 353-360 (1968).
72. Klein, U., Rajewsky, K. & KÃ¼ppers, R. Human Immunoglobulin (Ig)M+IgD+ Peripheral Blood B Cells Expressing the CD27 Cell Surface Antigen Carry Somatically Mutated Variable Region Genes: CD27 as a General Marker for Somatically Mutated (Memory) B Cells. *The Journal of Experimental Medicine* **188**, 1679-1689 (1998).
73. Morgan, J.W., Kouttab, N., Ford, D. & Maizel, A.L. Vitamin D-mediated gene regulation in phenotypically defined human B cell subpopulations. *Endocrinology* **141**, 3225-3234 (2000).
74. Cogswell, P.C., Scheinman, R.I. & Baldwin, A.S., Jr. Promoter of the human NF-kappa B p50/p105 gene. Regulation by NF-kappa B subunits and by c-REL. *J Immunol* **150**, 2794-2804 (1993).

75. Morgan, J.W., Sliney, D.J., Morgan, D.M. & Maizel, A.L. Differential regulation of gene transcription in subpopulations of human B lymphocytes by vitamin D3. *Endocrinology* **140**, 381-391 (1999).
76. Luger, E.O. *et al.* Induction of long-lived allergen-specific plasma cells by mucosal allergen challenge. *J Allergy Clin Immunol* **124**, 819-826 e814 (2009).
77. Metcalfe, D.D., Baram, D. & Mekori, Y.A. Mast cells. *Physiol Rev* **77**, 1033-1079 (1997).
78. Baeke, F., Takiishi, T., Korf, H., Gysemans, C. & Mathieu, C. Vitamin D: modulator of the immune system. *Curr Opin Pharmacol* **10**, 482-496 (2010).
79. Masoli, M., Fabian, D., Holt, S., Beasley, R. & Global Initiative for Asthma, P. The global burden of asthma: executive summary of the GINA Dissemination Committee Report. *Allergy* **59**, 469-478 (2004).
80. Andrew Aligne, C., Auinger, P., Byrd, R.S. & Weitzman, M. Risk Factors for Pediatric Asthma . Contributions of Poverty, Race, and Urban Residence. *Am. J. Respir. Crit. Care Med.* **162**, 873-877 (2000).
81. Hannan, M.T. *et al.* Serum 25-Hydroxyvitamin D and Bone Mineral Density in a Racially and Ethnically Diverse Group of Men. *J Clin Endocrinol Metab* **93**, 40-46 (2008).
82. Taher, Y.A., van Esch, B.C.A.M., Hofman, G.A., Henricks, P.A.J. & van Oosterhout, A.J.M. 1,25-Dihydroxyvitamin D3 Potentiates the Beneficial Effects of Allergen Immunotherapy in a Mouse Model of Allergic Asthma: Role for IL-10 and TGF-beta. *The Journal of Immunology* **180**, 5211-5221 (2008).
83. Larche, M., Akdis, C.A. & Valenta, R. Immunological mechanisms of allergen-specific immunotherapy. *Nat Rev Immunol* **6**, 761-771 (2006).
84. Bacharier, L.B. & Geha, R.S. Molecular mechanisms of IgE regulation. *J Allergy Clin Immunol* **105**, S547-558 (2000).
85. Snapper, C.M. *et al.* B cells from p50/NF-kappa B knockout mice have selective defects in proliferation, differentiation, germ-line CH transcription, and Ig class switching. *J Immunol* **156**, 183-191 (1996).
86. Sha, W.C., Liou, H.-C., Tuomanen, E.I. & Baltimore, D. Targeted disruption of the p50 subunit of NF-[kappa]B leads to multifocal defects in immune responses. *Cell* **80**, 321-330 (1995).
87. Dong, X. *et al.* Regulation of relB in dendritic cells by means of modulated association of vitamin D receptor and histone deacetylase 3 with the promoter. *Proc Natl Acad Sci U S A* **102**, 16007-16012 (2005).
88. Griffin, M.D., Dong, X. & Kumar, R. Vitamin D receptor-mediated suppression of RelB in antigen presenting cells: a paradigm for ligand-augmented negative transcriptional regulation. *Arch Biochem Biophys* **460**, 218-226 (2007).
89. Chung, J. *et al.* 1,25(OH)(2)D(3) blocks TNF-induced monocytic tissue factor expression by inhibition of transcription factors AP-1 and NF-kappaB. *Lab Invest* **87**, 540-547 (2007).
90. Sun, J. *et al.* Increased NF-kappaB activity in fibroblasts lacking the vitamin D receptor. *Am J Physiol Endocrinol Metab* **291**, E315-E322 (2006).
91. Ten, R.M. *et al.* The characterization of the promoter of the gene encoding the p50 subunit of NF-kappa B indicates that it participates in its own regulation. *EMBO J* **11**, 195-203 (1992).
92. Sun, J. *et al.* Lithocholic acid down-regulation of NF-kappaB activity through vitamin D receptor in colonic cancer cells. *J Steroid Biochem Mol Biol* **111**, 37-40 (2008).

93. Tse, A.K. *et al.* 1,25-dihydroxyvitamin D3 induces biphasic NF-kappaB responses during HL-60 leukemia cells differentiation through protein induction and PI3K/Akt-dependent phosphorylation/degradation of IkappaB. *Exp Cell Res* **313**, 1722-1734 (2007).
94. Riis, J.L. *et al.* 1alpha,25(OH)(2)D(3) regulates NF-kappaB DNA binding activity in cultured normal human keratinocytes through an increase in IkappaBalpha expression. *Arch Dermatol Res* **296**, 195-202 (2004).
95. Tan, X., Wen, X. & Liu, Y. Paricalcitol Inhibits Renal Inflammation by Promoting Vitamin D Receptor-Mediated Sequestration of NF-{kappa}B Signaling. *J Am Soc Nephrol* (2008).
96. Adams, L.S. & Teegarden, D. 1,25-Dihydroxycholecalciferol Inhibits Apoptosis in C3H10T1/2 Murine Fibroblast Cells Through Activation of Nuclear Factor kappaB. *J Nutr* **134**, 2948-2952 (2004).
97. Szeto, F.L. *et al.* Involvement of the vitamin D receptor in the regulation of NF-kappaB activity in fibroblasts. *J Steroid Biochem Mol Biol* **103**, 563-566 (2007).
98. Fagerlund, R., Kinnunen, L., Kohler, M., Julkunen, I. & Melen, K. NF-{kappa}B is transported into the nucleus by importin {alpha}3 and importin {alpha}4. *J Biol Chem* **280**, 15942-15951 (2005).
99. Fagerlund, R., Melen, K., Cao, X. & Julkunen, I. NF-kappaB p52, RelB and c-Rel are transported into the nucleus via a subset of importin alpha molecules. *Cell Signal* **20**, 1442-1451 (2008).
100. Suzuki, T. *et al.* Differentiation-associated alteration in gene expression of importins and exportins in human leukemia HL-60 cells. *Biomed Res* **29**, 141-145 (2008).
101. Basso, K. *et al.* Tracking CD40 signaling during germinal center development. *Blood* **104**, 4088-4096 (2004).
102. Lou, Y.R. *et al.* 25-Hydroxyvitamin D(3) is an agonistic vitamin D receptor ligand. *J Steroid Biochem Mol Biol* **118**, 162-170 (2010).
103. Shirakawa, A.K. *et al.* 1,25-Dihydroxyvitamin D3 Induces CCR10 Expression in Terminally Differentiating Human B Cells. *J Immunol* **180**, 2786-2795 (2008).
104. Yu, S., Bruce, D., Froicu, M., Weaver, V. & Cantorna, M.T. Failure of T cell homing, reduced CD4/CD8alphaalpha intraepithelial lymphocytes, and inflammation in the gut of vitamin D receptor KO mice. *Proc Natl Acad Sci U S A* **105**, 20834-20839 (2008).
105. Bromley, S.K., Thomas, S.Y. & Luster, A.D. Chemokine receptor CCR7 guides T cell exit from peripheral tissues and entry into afferent lymphatics. *Nat Immunol* **6**, 895-901 (2005).
106. Sallusto, F., Geginat, J. & Lanzavecchia, A. Central Memory and Effector Memory T Cell Subsets: Function, Generation, and Maintenance. *Annu Rev Immunol* **22**, 745-763 (2004).
107. Baeke, F. *et al.* The Vitamin D Analog, TX527, Promotes a Human CD4+CD25highCD127low Regulatory T Cell Profile and Induces a Migratory Signature Specific for Homing to Sites of Inflammation. *J Immunol* **186**, 132-142 (2011).
108. Jeffery, L.E. *et al.* 1,25-Dihydroxyvitamin D3 and IL-2 Combine to Inhibit T Cell Production of Inflammatory Cytokines and Promote Development of Regulatory T Cells Expressing CTLA-4 and FoxP3. *J Immunol* **183**, 5458-5467 (2009).
109. Dimeloe, S., Nanzer, A., Ryanna, K. & Hawrylowicz, C. Regulatory T cells, inflammation and the allergic response-The role of glucocorticoids and Vitamin D. *J Steroid Biochem Mol Biol* **120**, 86-95 (2010).

110. Gregori, S., Giarratana, N., Smiroldo, S., Uskokovic, M. & Adorini, L. A 1,25-Dihydroxyvitamin D3 Analog Enhances Regulatory T-Cells and Arrests Autoimmune Diabetes in NOD Mice. *Diabetes* **51**, 1367-1374 (2002).
111. Herz, U., Renz, H. & Wiedermann, U. Animal models of type I allergy using recombinant allergens. *Methods* **32**, 271-280 (2004).
112. Wittke, A., Weaver, V., Mahon, B.D., August, A. & Cantorna, M.T. Vitamin D receptor-deficient mice fail to develop experimental allergic asthma. *J Immunol* **173**, 3432-3436 (2004).
113. Overbergh, L. *et al.* Identification and immune regulation of 25-hydroxyvitamin D-1-α-hydroxylase in murine macrophages. *Clin Exp Immunol* **120**, 139-146 (2000).
114. Palmer, M.T. *et al.* Lineage-specific Effects of 1,25-Dihydroxyvitamin D3 on the Development of Effector CD4 T Cells. *J Biol Chem*.
115. Cantorna, M.T., Zhu, Y., Froicu, M. & Wittke, A. Vitamin D status, 1,25-dihydroxyvitamin D3, and the immune system. *Am J Clin Nutr* **80**, 1717S-1720S (2004).
116. Kreindler, J.L. *et al.* Vitamin D3 attenuates Th2 responses to Aspergillus fumigatus mounted by CD4+ T cells from cystic fibrosis patients with allergic bronchopulmonary aspergillosis. *J Clin Invest* **120**, 3242-3254 (2010).
117. Biswas, P. *et al.* 1,25-Dihydroxyvitamin D3 Upregulates Functional CXCR4 Human Immunodeficiency Virus Type 1 Coreceptors in U937 Minus Clones: NF-kappa B-Independent Enhancement of Viral Replication. *J. Virol.* **72**, 8380-8383 (1998).
118. Yoshida, T. *et al.* Memory B and memory plasma cells. *Immunological Reviews* **237**, 117-139 (2010).
119. Katz, H.R. *et al.* Secretory granule mediator release and generation of oxidative metabolites of arachidonic acid via Fc-IgG receptor bridging in mouse mast cells. *J Immunol* **148**, 868-871 (1992).
120. Kubach, J. *et al.* Dendritic cells: sentinels of immunity and tolerance. *Int J Hematol* **81**, 197-203 (2005).
121. Penna, G. & Adorini, L. 1alpha,25-Dihydroxyvitamin D3 Inhibits Differentiation, Maturation, Activation, and Survival of Dendritic Cells Leading to Impaired Alloreactive T Cell Activation. *J Immunol* **164**, 2405-2411 (2000).
122. Széles, L. *et al.* 1,25-Dihydroxyvitamin D3 Is an Autonomous Regulator of the Transcriptional Changes Leading to a Tolerogenic Dendritic Cell Phenotype. *J Immunol* **182**, 2074-2083 (2009).

10. ABBREVIATIONS

1α,25(OH)VD_3	1α,25-dihydroxyvitamin D_3, calcitriol
25(OH)VD_3	25-hydroxyvitamin D_3
7 aminoactinomycin D	7-AAD
AEC	33-Amino-9-ethyl-carbazole
AF-2	activation function-2
alum	$Al(OH)_3$, aluminiumhydroxide
AP	alkaline phosphatase
ASC	antibody secreting cell
bp	base pairs
Co-IP	Co-immunoprecipitation
DBD	DNA binding domain
DBP	vitamin D binding protein
DC	dendritic cell
dH_2O	distilled H_2O
DMF	N,N-dimethyl- formamide
DNA	deoxyribonucleic acid
ds	double-stranded
E	efficiency
FACS	fluorescence activated cell sorting
FGF23	fibroblast growth factor
FO	follicular B cells
for	forward primer
FSC	forward light scatter
HDAC	histone deacetylase
HPRT	hypoxanthine-guanine phosphoribosyltransferase
HRP	horseradish peroxidase
HSR	hypersensitivity reaction
Ig	immunoglobulin
IKK	inhibitor of κB kinase
IL	interleukin
i.p.	intraperitoneal
ko	knock out

LBD	ligand binding domain
LBP	ligand binding pocket
MACS	magnetic activated cell sorting
MZ	marginal zone B cells
NCoR	nuclear receptor corepressor
n.d.	not detectable
NEMO	NF-κB essential modulator
NF-κB	nuclear factor of κB
no.	number
NTP	nucleoside triphosphate
ORF	open reading frame
OVA	ovalbumin
PBMC	peripheral blood mononuclear cells
PBS	phosphate buffered saline
PCR	polymerase chain reaction
PDDR	pseudovitamin D-deficiency rickets
PFA	paraformaldehyde
PMT	photomultiplier tube
prom	promoter
PTH	parathyroid hormone
PVDF	polyvinylidenfluorid
rh	recombinant human
RT	reverse transcriptase
RXR	retinoid R receptor
SLE	systemic lupus erythematosus
SMRT	silencing mediator for retinoid and thyroid hormone receptors
SSC	side light scatter
T_H	T helper
TNFR	tumor-necrosis factor receptor
TRAF	TNFR associated factor
T_{reg}	regulatory T cells
Trpv6	transient receptor potential vanilloid type 6
UVB	ultraviolet B
VD	vitamin D

VD_3	vitamin D_3
VDIR	VDR interacting repressor
VDRE	vitamin D responsive element
wt	wild type

11. ACKNOWLEDGEMENTS

Als erstes möchte ich mich herzlich bei Professor Margitta Worm bedanken, die es mir ermöglicht hat, diese Arbeit in ihrer Gruppe durchzuführen. Sie unterstützte mich durch kontinuierliche wissenschaftliche Diskussionen und ermöglichte mir auch die Teilnahmen an Kongressen, um meine Daten zu präsentieren und neue Ideen zu entwickeln.

Desweiteren bedanke ich mich bei Dr. Guido Heine für die Einführung in die Welt des Vitamin D und zahlreiche Diskussionen zu diesem Thema.

Ich möchte mich bei Professor Roland Lauster für die Betreuung dieser Arbeit und viel Unterstützung gerade in der Endphase herzlich bedanken.

Danke an Dr. Magda Babina für viele praktische Hinweise zum Thema Proteinchemie und Immunpräzipitation.

Ein herzlicher Dank geht an Dr. Ria Baumgraß und Stefan Frischbutter für viel theoretische und praktische Hilfe zum Thema NF-κB. Ich bedanke mich für die Möglichkeit, die Techniken EMSA und Coimmunpräzipitation zu erlernen und für die Unterstützung bei der Analyse.

Ich bedanke mich herzlich bei Dennis Ernst für seine technische und moralische Unterstützung. Er war mir und meinen Mäusen immer eine unschätzbare Hilfe.

Danke an Juliane Lindner für großartige Unterstützung bei den murinen ELISAs und an Carolin Hobe für viel Hilfe bei der Separation naiver B-Zellen.

Ein besonderer Dank geht an meinen Büronachbarn Björn Hartmann für die Aufmunterung, wenn es mal nicht so lief, für wissenschaftliche Diskussionen und dafür, das er mir beigebracht hat, einen ganz brauchbaren Kaffee zu kochen.

Danke auch an Dr. Christin Weise, die immer bereit war, wissenschaftliche Probleme zu diskultieren und mir viele konstruktive Hinweise gab.

Danken möchte ich auch all meinen Kollegen für Unterstützung in unterschiedlichsten Situationen, für die schöne Zeit und Unmengen an Kuchen: Mandana Abdollahnia, Sabine Dölle, Gennadiy Drozdenko, Verena Fokuhl, Sven Guhl, Dana Hoser, Katharina Jörß, Pascal Klaus, Kiran Kumar, Vandana Kumari, Juliane Lindner, Milena Milovanovic, Maria Nassiri, René Riedel, Friederike Thiele und Yan Zhu.

Nicht zuletzt möchte ich mich ganz herzlich bei meiner Familie bedanken für die liebevolle Unterstützung während all meiner Hochs und Tiefs in den letzten 5 Jahren.